nature communications

Article

https://doi.org/10.1038/s41467-025-57306-7

The adaptor protein AP-3β disassembles heat-induced stress granules via 19S regulatory particle in *Arabidopsis*

Received: 15 July 2024

Accepted: 13 February 2025

Published online: 27 February 2025

Check for updates

Lei Pang, Yuanzhi Huang, Yilin He, Dong Jiang & Ruixi Li

To survive under adverse conditions, plants form stress granules (SGs) to temporally store mRNA and halt translation as a primary response. Dysregulation in SG disassembly can have detrimental effects on plant survival after stress release, yet the underlying mechanism remains poorly understood. Using Arabidopsis as a model system, we demonstrate that the β subunit of adaptor protein (AP) -3 complex (AP-3β) interacts with the SG core RNA-binding proteins Tudor staphylococcal nuclease 1/2 (TSN1/2) both in vitro and in vivo. We also show that AP-3β is rapidly recruited to SGs upon heat induction and plays a key role in disassembling SGs during stress recovery. Genetic evidences support that AP-3β serves as an adaptor to recruit the 19S regulatory particle (RP) of the proteasome to SGs. Notably, the 19S RP promotes SG disassembly through RP-associated deubiquitylation, independent of its proteolytic activity. This deubiquitylation process of SG components is crucial for translation reinitiation and growth recovery after heat release. Our findings uncover a previously unexplored role of the 19S RP in regulating SG disassembly and highlights the importance of endomembrane proteins in supporting RNA granule dynamics in plants.

Plants are constantly subjected to fluctuating environment and face various biotic and abiotic stresses. To survive under unfavorable conditions, plants have evolved diverse strategies to adjust growth and metabolisms. One important strategy is the formation of stress granules (SGs), the membraneless compartments that temporarily store and safeguard mRNA-ribosome complexes from degradation during stress conditions[1–3]. When stress is alleviated, SGs are disassembled, enabling mRNA release and the resumption of translation initiation. Dysfunction in SG disassembly can hinder post-stress growth recovery[4,5]. Therefore, unravelling the mechanism for SG disassembly could provide insights into critical aspects of cellular viability. An early study on fission yeast demonstrated that SG clearance is regulated through both autophagy and the p97/Cdc48/VCP-dependent mechanism[6]. Subsequent research in mammalian cells revealed that the 26S proteasome promotes SG clearance via its proteolytic function[7,8]. More recent studies have shown context-specific ubiquitylation profiles in mammalian SGs, which vary depending on the stress stimuli[9–11]. Rather than reflecting the capacity for degradation, heat-induced ubiquitylation primes cells to dismantle SGs and reinitiate normal cellular activities after stress release[9]. Recently, the HaloTag-based μMap platform (HaloMap) technology has uncovered the enrichment of K63-linked polyubiquitin chains in SG components, which are subsequently targeted by the autophagy-related pathway for granule clearance[12]. Therefore, autophagy, p97/Cdc48/VCP and 26S proteasome have all been identified as regulators for SG disassembly in different systems[6,8,11]. Regarding ubiquitin, despite being identified as the primary post-translational modification (PTM) in SG components, different studies have revealed distinct effectors that recognize this tag[9,12].

The mechanism for SG disassembly in plants, however, remains largely unexplored. In model plant *Arabidopsis*, several key RNA binding proteins (RBPs) have been identified as critical components of SGs in response to heat stress. These include Tudor staphylococcal nuclease (TSN)[13], RNA-binding protein 47 (RBP47)[14], Poly (A)-binding

Shenzhen Key Laboratory of Plant Genetic Engineering and Molecular Design, Institute of Plant and Food Science, Department of Biology, School of Life Sciences, Southern University of Science and Technology, Shenzhen 518055, China. e-mail: lirx@sustech.edu.cn

proteins (PABs)[15], Oligouridylate binding protein 1 (UBP1)[16], Acetylation lowers binding affinity (ALBA)[17], RNA-binding glycine-rich D2 (RBGD2) and RBGD4[18]. Although autophagy and 26S proteasome have been reported to play crucial roles in promoting SG disassembly in yeast and mammalian cells as outlined above, it remains unclear whether these mechanisms are conserved in plant system. There is currently no definitive evidence to suggest that autophagy facilitates SG disassembly in plant cells. As for the 26S proteasome, the existing knowledge presents contradictory aspects. An early study reported that the molecular chaperone heat shock protein (HSP) 101 interacts with the proteasome and promotes the clearance of ubiquitylated protein aggregates via its disaggregase activity[19]. Although many HSP101 clients are SG components, these targets are destined for refolding independent of the proteasome's proteolytic activity during heat recovery[19]. However, a recent study showed that the 26S proteasome, as a stable component of SGs, promotes the clearance of RBP47b-positive SGs through proteolysis during stress recovery[20]. Therefore, the precise role of the proteasome in regulating SG disassembly in plants remains to be determined.

The adaptor protein (AP) -3, is an evolutionarily conserved multisubunits complex composed of two large subunits (δ and β), one medium subunit (μ) and one small subunit (σ)[21]. In mammalian cells, AP-3 subunits are observed to localize to both the trans-Golgi network (TGN) and endosomal subdomains, and regulates cargo transport from the TGN or endosomes to lysosomes or lysosome-related organelles (LROs), bypassing the conventional multivesicular body (MVB)-based trafficking route[22,23]. In *Arabidopsis*, single copy of AP-3 subunits has been identified based on sequence similarity[24,25]. They also regulate the transport of cargoes to the vacuole bypassing MVBs[26], similar to the reported role of AP-3 complex in yeast and mammalian cells. However, the AP-3β subunit in *Arabidopsis* does not show obvious colocalization with known organelle markers[25], suggesting that this protein may have additional functions. Furthermore, the AP-3β null-mutants show no obvious growth defects[25]. Therefore, the potential biological functions of AP-3β in plants merit further investigation.

In this study, we report a role for AP-3β in regulating SG disassembly. Upon heat induction, AP-3β is rapidly recruited to SGs via its interaction with the SG core RBPs, TSN1/2. We also demonstrate that AP-3β acts as an adaptor, recruiting the 19S RP subunits to SGs. Notably, K63- but not K48-linked ubiquitylated proteins are highly enriched in heat-induced SGs, which are targeted by the 19S RP-associated deubiquitinases for SG disassembly. Our findings unveil an important role of the 19S RP in promoting SG disassembly and emphasize the significance of endomembrane system in guiding RNA granule dynamics in plants.

Result

AP-3β interacts with the SG core RNA-binding proteins TSN1/2

To investigate the biological roles of AP-3β in *Arabidopsis*, we carried out immuno-precipitation (IP) experiment coupled with mass spectrometry (IP-MS) to analyze the interaction proteins using *UBQ-GFP* transgenic plants as the negative control. In addition to successfully identifying the other three AP-3 subunits with high scores, we also found several RNA binding proteins (RBPs) enriched in the interactome with fold enrichment (FC) $Log_2FC_{AP\text{-}3\beta\text{-}GFP/UBQ\text{-}GFP} \geq 1$ (Fig. 1a and Supplementary Data S1). Among the RBPs, Tudor staphylococcal nuclease (TSN)2 was at the top in the list [$Log_2FC_{AP\text{-}3\beta\text{-}GFP/UBQ\text{-}GFP} = 3.17$, $-Log_{10}(P\text{-value}) = 1.91$) (Supplementary Data S1). TSN2 and its close homolog TSN1 are reported to be the SG core RBPs and form scaffold platform for SG assembly and growth[13,27]. The interaction between AP-3β and TSN1/2 was first confirmed by reciprocal coimmunoprecipitation (co-IP) in vivo. To do this, we generated two antibodies that specifically recognized AP-3β or TSN1/2 (Supplementary Fig. 1). TSN1/2 co-immunoprecipitated with AP-3β-GFP in vivo (Fig. 1b), consistent with the IP-MS data. In contrast, TSN2 failed to co-precipitate with VPS41, the subunit of homotypic fusion and vacuole protein sorting (HOPS) complex, although VPS41 is also an endomembrane protein[28] (Supplementary Fig. 2a). In a reciprocal experiment, AP-3β co-precipitated with the TSN1/2-GFP fusion protein but not the control free GFP (Fig. 1b). The interaction is specific, as AP-3β did not co-precipitate with PAB2, the other SG core RBP (Supplementary Fig. 2b).

To further confirm the interaction between AP-3β and TSN1/2, we performed luciferase complementation imaging (LCI) experiments via transient infiltration in *N. benthamiana* epidermal leaves. As a positive control, the combination between AP-3β and AP-3δ reconstituted strong luciferase activity. No luciferase signal was observed when Cluc-TSN1/2 was combined with empty Nluc or when AP-3β-Nluc was combined with empty Cluc, indicating the system worked well as expected. In accordance with the results from co-IP, AP-3β interacted with TSN1/2 but not with PAB2 in the LCI assays (Fig. 1c and Supplementary Fig. 2c). This result was further validated by bimolecular fluorescence complementation (BiFC) assays. We detected strong reconstituted YFP signals in cells coexpressing *AP-3β* and *TSN1/2* (Fig. 1d), but no obvious signal was observed in the coexpression pairs of *TSN1/2* and *VPS41* (Supplementary Fig. 2d), or *AP-3β* and *PAB2* (Supplementary Fig. 2e), further confirming the specificity of the interaction between AP-3β and TSN1/2. Finally, we demonstrated that the GST-tagged AP-3β protein directly interacted with the MBP-tagged TSN1/2 proteins through in vitro pull-down assays (Fig. 1e).

Taken together, these results suggest that AP-3β specifically interacts with TSN1/2 both in vitro and in vivo.

AP-3β is specifically recruited to SGs upon heat induction

It was reported that TSN1/2 are rapidly induced to form SGs under salt and heat stress[13,29]. Therefore, we further investigated whether AP-3β responds to stress stimuli similarly to TSN1/2. TSN2 was strongly induced under heat stress and mildly responded to NaCl treatment, with no response under osmotic stress. No changes were observed in free GFP protein. Interestingly, AP-3β was strongly induced and translocated to bright foci under heat stress, with no obvious changes after NaCl or mannitol treatment (Supplementary Fig. 3a).

We next analyzed the identity of heat-induced AP-3β foci by crossing with transgenic lines harboring different organelle marker proteins, including the Golgi marker SYP32[30], the TGN marker VAMP721[31], and the autophagosome marker ATG8e[32]. We also analyzed the co-localization between AP-3β and the styryl dye FM4-64, which traces endocytic vesicles from plasma membrane to the vacuole[33]. Heat induced strong aggregation of VAMP721, SYP32 and FM dye-labeled vesicles (Fig. 2a, c, Supplementary Fig. 3b). However, none of these aggregates showed obvious colocalization with the AP-3β-positive foci (Fig. 2a–d, Supplementary Fig. 3b, d). ATG8e did not colocalize with AP-3β or formed aggregates before and after heat treatment (Supplementary Fig. 3c, e). These results suggest that the heat-induced AP-3β foci do not colocalize with the conventional organelles.

The interaction between AP-3β and TSN1/2, as well as the response of AP-3β to heat stress, prompted us to further examine the relationship between AP-3β and SG markers. Remarkably, the heat-induced AP-3β foci strongly colocalized with both TSN2- and RBP47b-labeled SGs with high co-efficiency (Fig. 2e–h). We also compared the kinetics of AP-3β foci with TSN2-labeled SGs during heat induction. While TSN2 rapidly responded to heat stress and assembled into SGs around 5 min after the onset of heat induction, the AP-3β foci were induced slightly later and were first visualized around 10 min. After 15 min's heat induction, these foci were almost completely colocalized with TSN2-labled SGs (Supplementary Fig. 3f–i). This result was further confirmed by treating with the protein synthesis inhibitor cycloheximide (CHX), which inhibits polysome disassembly and disrupts SG formation[34]. Pretreatment with CHX completely blocked the induction of SGs, and no AP-3β foci were observed after heat stress (Fig. 2e–h), indicating that the induction of AP-3β foci depends on SGs assembly. The sequestration of AP-3β to SGs

https://doi.org/10.1038/s41467-025-57306-7

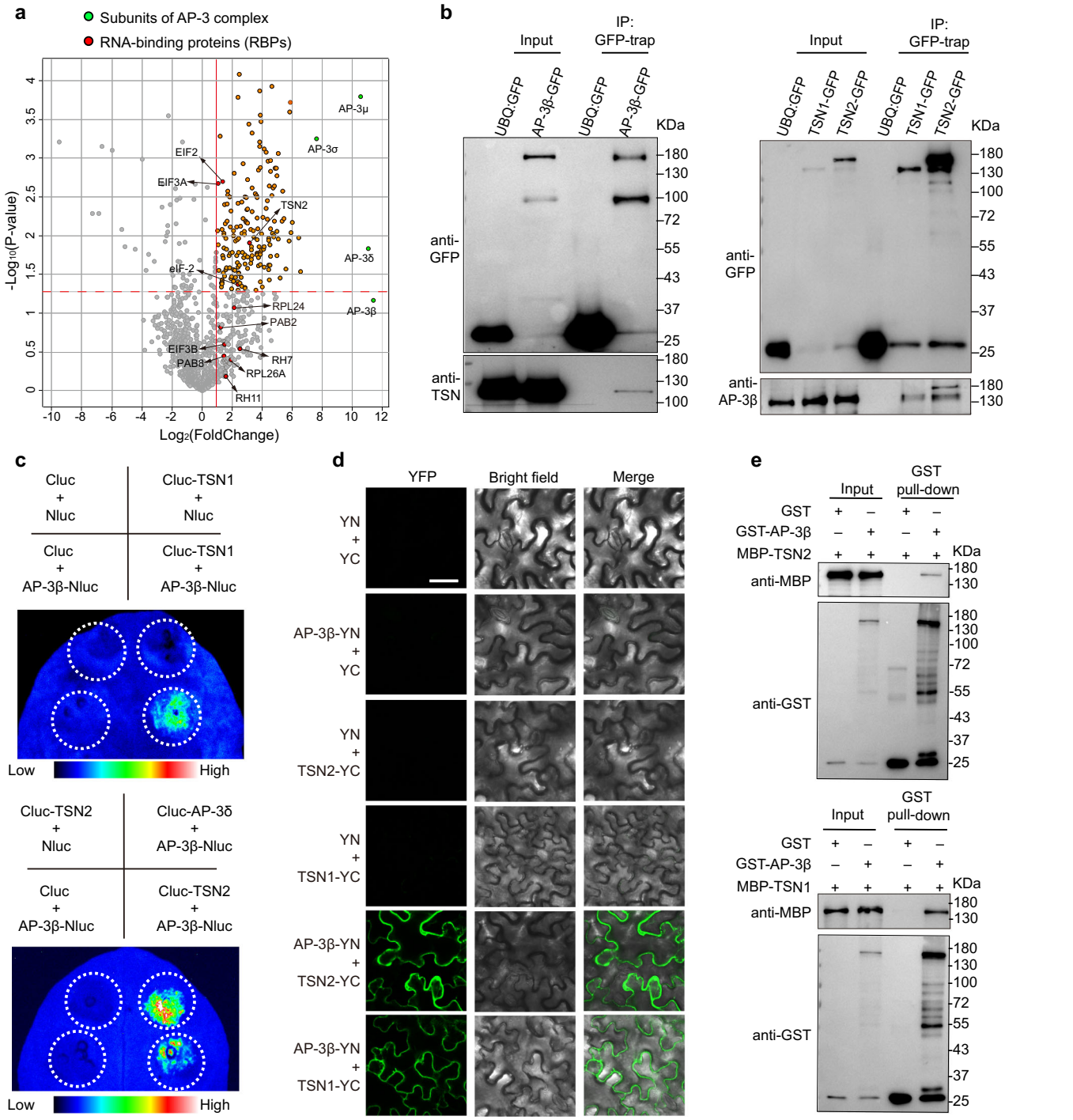

Fig. 1 | AP-3β interacts with the TSN1/2 proteins in vivo and in vitro. a Volcano plot illustrates the enrichment of proteins co-purified with AP-3β-GFP compared to the free GFP control. The X-axis represents the Log_2 fold change ($FC_{AP\text{-}3\beta\text{-}GFP/UBQ\text{-}GFP}$), while the Y-axis represents the $-Log_{10}$ (*P*-value). Proteins with a *P*-value < 0.05, indicated by the horizontal dashed red line, are considered significantly enriched. Statistical analysis was performed using a two-tailed unpaired Student's *t* test. The vertical red line indicates $Log_2FC = 1$. Proteins enriched with AP-3β that have a $Log_2FC \geq 1$ and *P*-value < 0.05 are highlighted in orange. The green and red circles represent the subunits of AP-3 complex and RNA-binding proteins (RBPs), respectively. **b** Reciprocal co-immunoprecipitation (Co-IP) assays demonstrate that AP-3β interacts with TSN1 and TSN2 in vivo. **c** Split-luciferin complementation imaging (LCI) assays reveal the interaction between AP-3β and TSN1 or TSN2. The interaction between AP-3β and AP-3δ served as a positive control. Dotted circles indicate the sample injection sites. **d** Bimolecular fluorescence complementation (BiFC) assays further consolidate the interaction between AP-3β and TSN1 or TSN2. Scale bars: 50 μm. **e** In vitro pull-down experiments demonstrate that AP-3β directly interacts with TSN1 and TSN2 proteins. Images in (**c**, **d**) were taken in infiltrated tobacco leaves. Images shown are representative of three independent biological experiments. Source data are provided as a Source Data file.

could be observed in root meristem and transition zone as well as the maturation zone in both young (3 d, 5 d) and older (10 d) seedlings (Supplementary Fig. 3j, k), indicating that this might be a universal phenomenon.

We further investigated whether the heat response of AP-3β depends on the AP-3 complex. However, AP-3δ failed to interact with TSN1/2 in LCI assays (Supplementary Fig. 4a, b). Moreover, AP-3β still fully colocalized with the TSN2-labeld SGs upon heat induction in AP-

https://doi.org/10.1038/s41467-025-57306-7

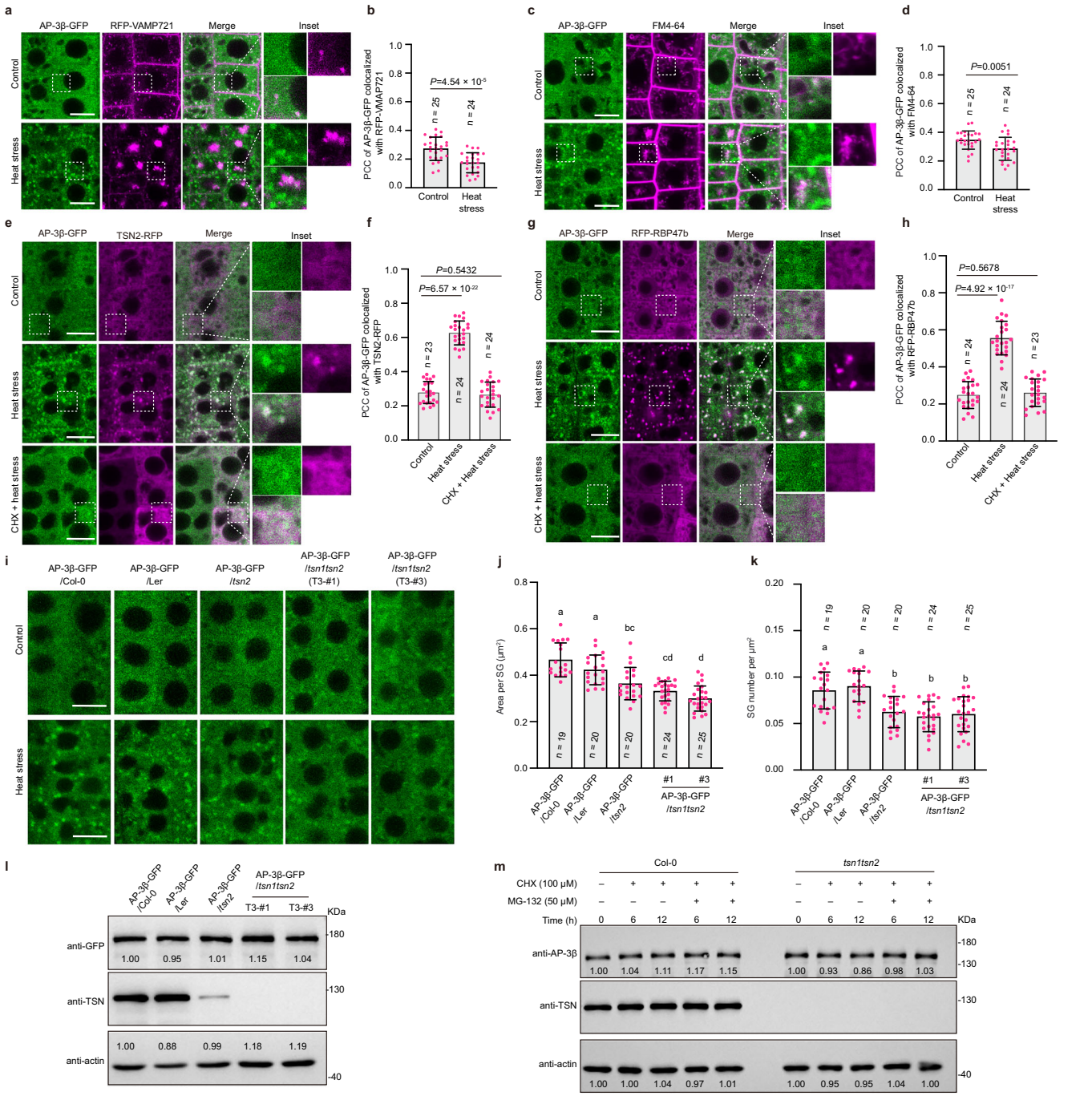

Fig. 2 | AP-3β is recruited to stress granules (SGs) upon heat induction. AP-3β does not show obvious colocalization with the TGN marker VAMP721 (**a**) or FM4-64-labeled endocytosic vesicles (**c**) under normal conditions (control) or after heat stress (39 °C, 40 min). Scale bars: 10 μm. Insets show enlarged views of the boxed regions. The colocalization between AP-3β and VAMP721 (**b**) or FM4-64 (**d**) was quantified using Pearson correlation coefficients (PCC). **e**, **g** Under control, AP-3β, TSN2 and RBP47b primarily distribute in the cytoplasm. Upon heat induction, AP-3β form many foci that are fully colocalized with the TSN2- (**e**) or RBP47b-labeled SGs (**g**). Pretreatment with cycloheximide (CHX) for 1 h completely abolishes SG assembly and the sequestration of AP-3β into SGs. Scale bars: 10 μm. Insets show enlarged views of the boxed regions. **f**, **h** The colocalization between AP-3β and TSN2 (**e**) or RBP47b (**g**) was quantified using PCC. **i** The sequestration of AP-3β to SGs after heat stress is reduced in *tsn1* single mutant and *tsn1tsn2* double mutant. Scale bars: 10 μm. Quantification of the size (**j**) and number (**k**) of AP-3β-positive foci after heat induction. **l** Immunoblot analysis reveals the protein level of AP-3β-GFP or TSN in different genotypes using anti-GFP or anti-TSN antibodies. The anti-actin antibody served as a loading control in parallel. **m** Immunoblot analysis shows that protein stability of AP-3β remains largely unchanged in *tsn1tsn2* double mutant compared to the Col-0 seedlings. For **b**, **d**, **f**, **h**, **j**, **k**, data represent mean ± SD from three independent biological experiments. For **b**, **d**, **f**, **h**, statistical analysis was performed using a two-tailed unpaired Student's *t* test; for **j**, **k**, statistical analysis was performed using one-way ANOVA with Tukey's multiple comparison test and different letters above the bars indicate statistical significance at $p < 0.05$. All confocal images were taken in the root meristem or transition zone of 5-day-old seedlings. Images are representative of three independent biological experiments. Source data are provided as a Source Data file.

3δ null-mutant *pat4-2*[24] and *ap-3μ-3* mutant[35] (Supplementary Fig. 4c, d), suggesting that AP-3β is recruited to SGs independent of the AP-3 complex. In contrast, the induction of AP-3β foci were significantly reduced in *tsn1tsn2* double mutants after heat stress (Fig. 2i–l), indicating that the proper function of TSN1/2 is essential for recruiting AP-3β to SGs. We also demonstrated that the protein abundancy of AP-3β was not obviously changed in *tsn1tsn2* double mutants after cycloheximide (CHX) treatment in the presence or absence of MG-132 (Fig. 2m), suggesting its reduced distribution in SGs of *tsn1tsn2* mutants is not caused by protein instability.

In summary, we conclude that AP-3β specifically responds to heat stress and is rapidly recruited to SGs through its interaction with TSN1/2 proteins.

The AP-3β-positive SGs are associated with membrane and show overlap with the processing bodies (PBs)

Intriguingly, we frequently observed the plasma membrane (PM) distribution of AP-3β after heat stress. Although AP-3β was found to colocalize with both TSN2- and RBP47b-labeled SGs at intracellular foci, its colocalization at the PM was only observed with TSN2 (Supplementary Fig. 5a–c). We further probed the dynamics of AP-3β using fluorescent recovery after photo bleach (FRAP), and compared with TSN2 and RBP47b. While the RBP47b-positive SGs rapidly recovered after photobleach, TSN2-labeled SGs remained unchanged under the same condition (Supplementary Fig. 5d), similar to previous reports[13]. Notably, the AP-3β foci also could not recover after photobleach (Supplementary Fig. 5d). This result suggests that membrane-associated and liquid-like SGs coexist in plant cells upon heat induction.

SGs have a close relationship with the PBs[1,36]. It is worth noting that heat stress also triggered the colocalization of AP-3β-positive foci with DCP5-labeled PBs[37] (Supplementary Fig. 5e, f), indicating that AP-3β is recruited to both SGs and PBs following heat induction. However, the AP-3β null-mutant *pat2-2*[25] did not significantly affect the stability of PB-targeted RNAs after heat stress, unlike the typical PB mutant *dcp5-1* (Supplementary Fig. 5g). This implies that AP-3β may not be the primary regulator of PB function.

AP-3β is recruited to SGs depending on its interaction with TSN1/2 and membrane-association characteristics

As an evolutionarily conserved AP-3 subunit, AP-3β's sequestration to SGs is unexpected. Therefore, we analyzed which domain was responsible for its unique role in heat response. AP-3β consists two functional domains: the N-terminal adaptor domain (40-639 aa) and the C-terminal AP3β_C domain (795-947 aa) (Fig. 3a). An intrinsically disordered region lies between the two domains (IDR) (717-791 aa) (Fig. 3a, predicted by the IUPred3 program, https://iupred3.elte.hu/). We therefore generated four truncated proteins: AP-3β_C without the N-terminus, AP-3β_N without the C-terminus, AP-3βΔAP3β_C without the C-terminal AP3β_C domain, and AP-3βΔIDR without the IDR domain. Using BiFC and LCI assays, we showed that the N-terminal adaptor domain was required for the interaction between AP-3β and AP-3δ, while the C-terminal AP3β_C domain determined its interaction with TSN2. The IDR domain was dispensable for any of the interactions (Fig. 3b, c, Supplementary Fig. 6a–c). These results were further corroborated by an in vitro pull-down assay, which showed a strong interaction between TSN2 and AP-3β_C domain but not AP-3β_N domain (Fig. 3d). Therefore, AP-3β is integrated into AP-3 complex through the N-terminal adaptor domain but interacts with TSN2 via the C-terminal AP3β_C domain.

To investigate which domain is responsible for the heat response of AP-3β, we generated three transgenic lines harboring the genomic fragment of AP-3β without the C-terminal AP3β_C domain (AP-3βΔAP3β_C-GFP) or the IDR region (AP-3βΔIDR-GFP) or the N-terminal adaptor domain (AP-3βΔN-GFP) in the background of *pat2-2* mutant. Transgenic plants with the full-length genomic fragment (AP-3β-GFP) were used as a positive control. All the complementation lines were crossed with the SG marker TSN2-RFP or the TGN marker RFP-VAMP721 and analyzed in the F3 homozygous progeny. The AP-3β full-length protein seldom colocalized with VAMP721 at room temperature but was rapidly recruited to TSN2-labled SGs upon heat induction (Fig. 3e–h), similar to our previous results (Fig. 2). The AP-3βΔIDR truncated protein displayed a similar response as the full-length protein before and after heat stress (Fig. 3i–l). Strikingly, the AP-3βΔAP3β_C truncated protein increased colocalization with VAMP721 under normal condition but significantly reduced the colocalization with SGs after heat treatment. Instead, it formed many aggregates upon heat induction, which prominently colocalized with VAMP721 (Fig. 3m–p). These findings suggest that the AP3β_C domain is required for recruiting AP-3β to SGs; without it, the protein is translocated to VAMP721-labeled TGN. The AP-3βΔN protein obviously increased its distribution in the cytoplasm, which was further confirmed by membrane fractionation (Supplementary Fig. 6d–g). As expected, the AP-3βΔN protein failed to interact with AP-3δ but coprecipitated with TSN2 in vivo (Supplementary Fig. 6h). Interestingly, the AP-3βΔN protein did not respond to heat stress, showing no obvious colocalization with either VAMP721-labled TGN or TSN2-positive SGs (Fig. 3q–t), indicating that the membrane-association property of AP-3β is also important for its sequestration into SGs.

In summary, we conclude that the AP3β_C domain governs the interaction of AP-3β with TSN1/2, while the N-terminal adaptor domain is vital for the assembly of AP-3 complex and its distribution in endomembrane system. Both domains are necessary for recruiting AP-3β to SGs following heat stress.

AP-3β is crucial for SG disassembly and growth restore during heat recovery

We conducted further investigations to analyze whether AP-3β regulates SG dynamics. Consistent with the previous report[13], the TSN2-positive SGs were rapidly induced around 10 min after heat induction, gradually enriched at bright foci alongside heat induction, and reached maximum intensity around 30 min (Fig. 4a). The percentage of cells with SGs at different time points was similar in *pat2-2* compared to control seedlings (Fig. 4a, b), although the size of SGs was slightly reduced in the mutant at late stage of SG induction (Fig. 4c), indicating that AP-3β plays a minor role in regulating SG assembly. In contrast, the disassembly of SGs was significantly delayed in *pat2-2* mutant. In control seedlings, SGs were disassembled in 40% of the cells after the onset of recovery, cleared in more than 80% of cells around 5 h and disappeared in most cells around 6 h (Fig. 4d, e). In *pat2-2* mutants, however, more than 80% of cells still contained SGs at 4 h after heat removal. The difference became more pronounced at 5 h, when SGs were still observed in about 60% of cells in *pat2-2* mutants, while less than 20% of cells in control seedlings contained SGs at the same time (Fig. 4d, e). These data suggest that AP-3β preferentially regulates SG disassembly during heat recovery. In contrast, the AP-3δ mutant *pat4-2* did not significantly impair SG disassembly, and the *pat2-2 pat4-2* double mutant showed a similar recovery rate as the *pat2-2* single mutant (Supplementary Fig. 7), suggesting that AP-3β is the primary regulator for SG disassembly within the AP-3 complex.

We next investigated the physiological role of AP-3β in heat response, using the heat-sensitive chaperon mutant *hsp101*[19] as a positive control. The *pat2-2* mutants displayed hypersensitivity to heat stress, significantly reducing their survival rate (Supplementary Fig. 8). Complementation with the full-length AP-3β protein fully restored the growth defects in *pat2-2* mutants after heat stress. However, both the AP-3βΔAP3β_C and AP-3βΔN truncated proteins failed to rescue the heat-sensitive defects in *pat2-2* mutants (Fig. 4f–i, Supplementary Fig. 8), supporting the notion that the proper function of AP-3β is essential for plant growth recovery after heat stress.

https://doi.org/10.1038/s41467-025-57306-7

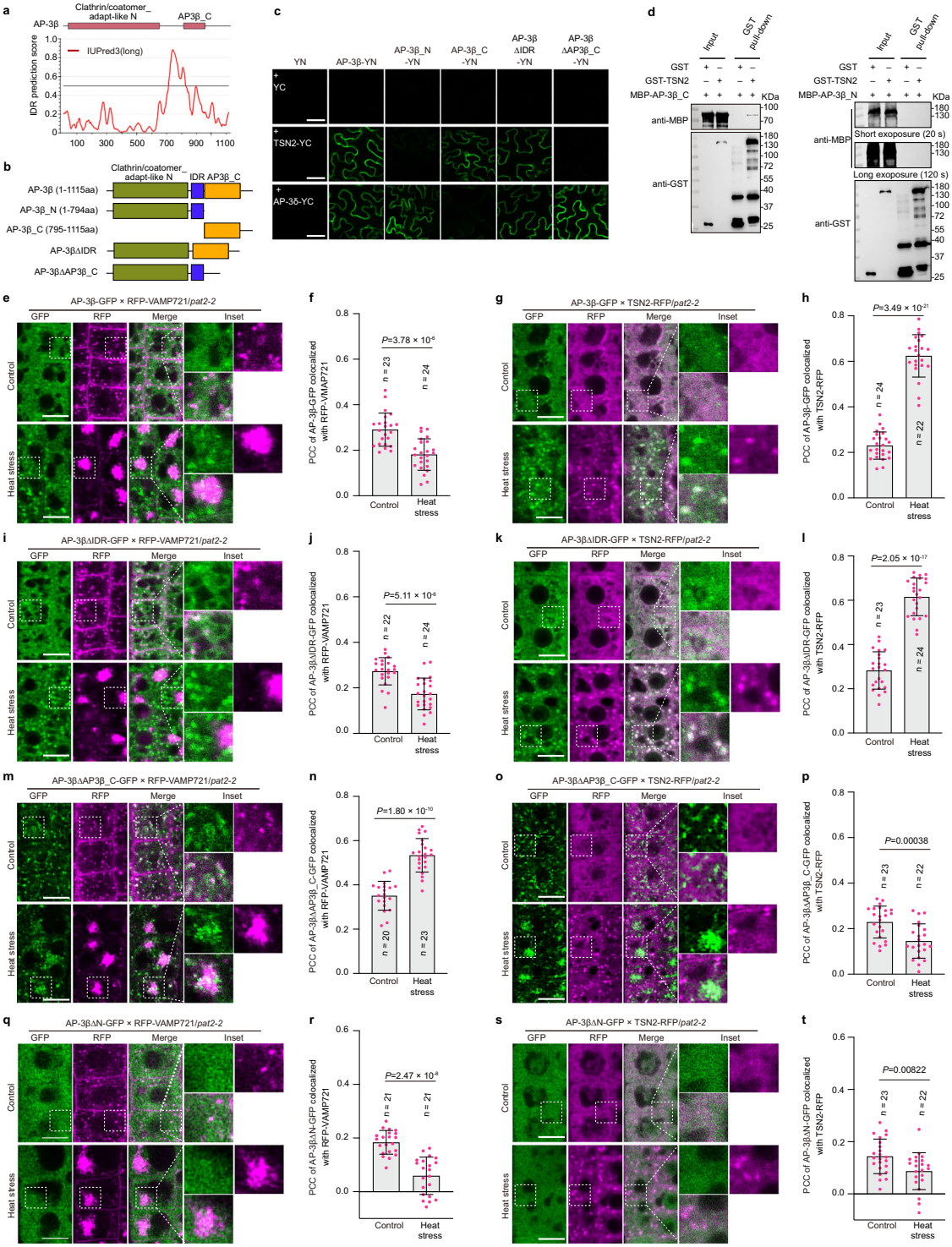

Fig. 3 | AP-3β is recruited to SGs depending on its interaction with TSN1/2 and membrane-association property. a Schematic map of the AP-3β protein and prediction of intrinsically disordered regions (IDRs) using online software IUPred 3. **b** Schematic diagram of the AP-3β truncated proteins. **c** BiFC assays reveal that AP-3β interacts with AP-3δ through the N-terminal adaptor domain, while the C-terminal AP3β_C domain determines its interaction with TSN2; the IDR domain is dispensable for any of the interactions. Scale bars: 50 μm. **d** Pull-down assays support that the C-terminus of AP-3β directly interacts with TSN2 while the N-terminus shows no interaction. Representative images showing the subcellular colocalization pattern between the TGN marker RFP-VAMP721 and AP-3β-GFP (**e**), AP-3βΔIDR-GFP (**i**), AP-3βΔAP3β_C-GFP (**m**) or AP-3βΔN-GFP (**q**). Insets show enlarged views of the boxed regions. Scale bars: 10 μm. The colocalization between RFP-VAMP721 and AP-3β-GFP (**f**), AP-3βΔIDR-GFP (**j**), AP-3βΔAP3β_C-GFP (**n**) or AP-3βΔN-GFP (**r**) were quantified using PCC. Representative images showing the subcellular colocalization pattern between the SG marker TSN2-RFP and AP-3β-GFP (**g**), AP-3βΔIDR-GFP (**k**), AP-3βΔAP3β_C-GFP (**o**) or AP-3βΔN-GFP (**s**). Insets show enlarged views of the boxed regions. Scale bars: 10 μm. The colocalization between TSN2-RFP and AP-3β-GFP (**h**), AP-3βΔIDR-GFP (**l**), AP-3βΔAP3β_C-GFP (**p**) or AP-3βΔN-GFP (**t**) were quantified using PCC. For **f**, **j**, **n**, **r**, **g**, **k**, **o** and **s**, data represent mean ± SD from three independent biological experiments; statistical analysis was performed using a two-tailed unpaired Student's *t* test. All confocal images except (**c**) were taken in the root meristem or transition zone of 5-day-old seedlings; images in (**c**) were taken in infiltrated tobacco leaves. All images are representative of three independent biological experiments. Source data are provided as a Source Data file.

https://doi.org/10.1038/s41467-025-57306-7

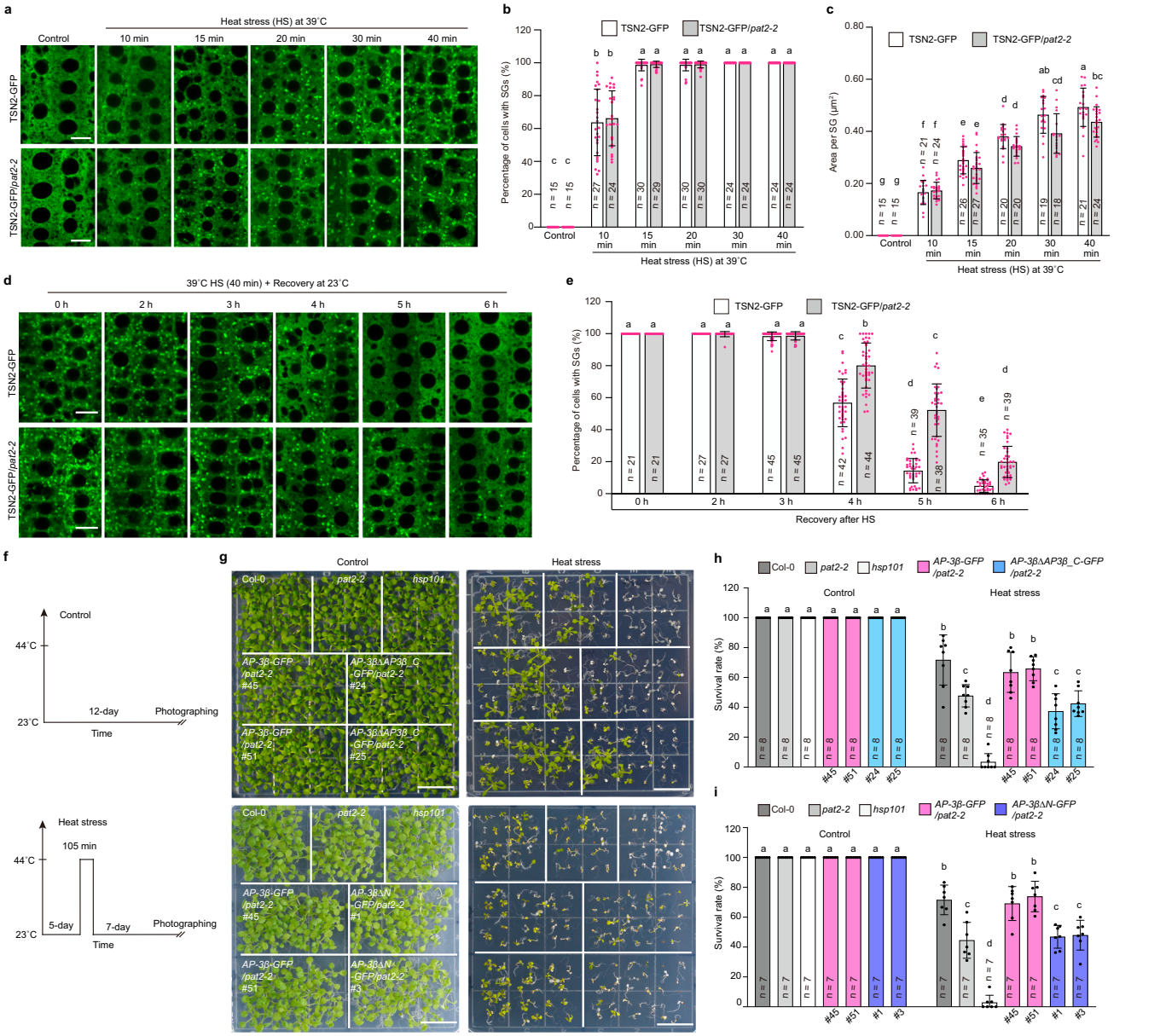

Fig. 4 | Dysfunction in AP-3β delays SGs disassembly and reduces plant survival rate after heat stress. a The TSN2-positive SGs are induced at similar level in *pat2-2* mutant compared to Col-0 control seedlings at different time points during heat induction. Scale bars: 10 μm. Quantification of the percentage of cells with SGs (**b**) and the size of SGs (**c**) at different time points as shown in (**a**). Data represent mean ± SD from three independent biological experiments. **d** The disassembly of SGs was significantly delayed in *pat2-2* mutant after heat stress release. Scale bars: 10 μm. **e** Quantification of the percentage of cells with SGs at different time points as shown in (**d**). Data represent mean ± SD from three independent biological experiments. **f** Schematic diagram of heat stress assays. **g** The *pat2-2* mutants significantly reduce the survival rate after heat stress. Complementation with the full-length AP-3β protein fully restores the growth defects in *pat2-2* mutants after heat stress; however, both the AP-3βΔAP3β _C and AP-3βΔN truncated proteins fail to rescue the heat-sensitive defects. The *hsp101* mutant was used as a positive control. Scale bars: 1.5 cm. **h**, **i** Quantification of the plant survival rate as shown in (**g**). Data represent mean ± SD from at least seven independent biological experiments with at least 30 seedlings for each genotype per replicate. Confocal images in (**a**, **d**) were taken in the root meristem or transition zone of 5-day-old seedlings. For **b**, **c**, **e**, **h**, **i**, statistical analysis was performed using one-way ANOVA with Tukey's multiple comparison test and different letters above the bars indicate statistical significance at $P < 0.05$. Source data are provided as a Source Data file.

In conclusion, our findings indicate that AP-3β is instrumental for SG disassembly and plant growth recovery after heat release.

AP-3β selectively recruits the 19S regulatory particle (RP) subunits of the proteasome to SGs upon heat induction

We next explored the mechanism by which AP-3β regulates SG disassembly. We first demonstrated that autophagy was dispensable for disassembling the heat-induced SGs, as the autophagosome marker ATG8 was not recruited to SGs after heat induction and SGs disassembled at similar kinetics in canonical autophagy mutant *atg7* (Supplementary Fig. 9). This is distinct from the reported mechanism in yeast and mammalian cells[6,38]. Interestingly, apart from the RBPs, we also identified many proteasome subunits in the interactome of AP-3β ($Log_2FC_{AP\text{-}3\beta\text{-}GFP/UBQ\text{-}GFP} \geq 1$) (Supplementary Data S1). The 26S proteasome is a large complex consisting of two subcomplexes: the 19S regulatory particle (RP) and 20S core particle (CP). Co-IP analysis revealed that the 19S RP but not 20S CP subunits co-precipitated with AP-3β before and after heat stress (Fig. 5a). We also proved that AP-3β interacted with the RPT2a and RPT2b subunits by yeast-two-hybrid assays (Fig. 5b). This was further confirmed by in vitro co-IP. GST-

https://doi.org/10.1038/s41467-025-57306-7

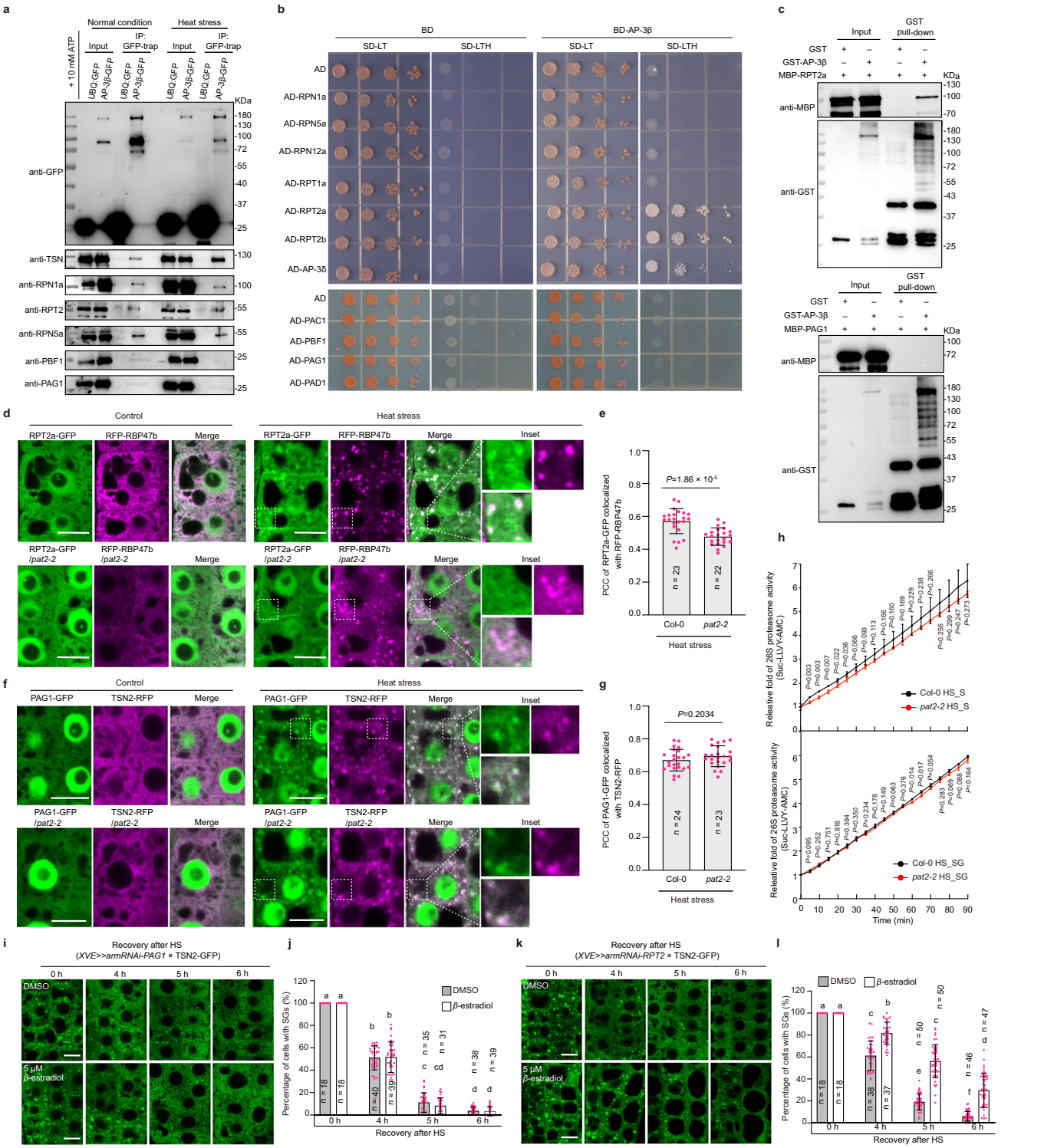

Fig. 5 | AP-3β acts as an adaptor to recruit the 19S RP subunits to SGs upon heat stress. a Co-IP assays reveal that AP-3β preferentially interacts with the 19S RP subunits but not 20S CP subunits under control or after heat stress. **b** Yeast two-hybrid assays demonstrate that AP-3β specifically interacts with the 19S RP subunits RPT2a and RPT2b. The interaction between AP-3β and AP-3δ was used as a positive control. **c** In vitro pull-down assays demonstrate that AP-3β interacts with RPT2a but not with PAG1. Both the RP subunit RPT2a and CP subunit PAG1 are recruited to RBP47b- or TSN2-labeled SGs upon heat induction (**d**, **f**). However, the *pat2-2* mutant disrupts the sequestration of RPT2a (**d**) but not PAG1 (**f**) to SGs. Insets show enlarged views of the boxed regions. Scale bars: 10 μm. Quantification of the colocalization between RPT2a and RBP47b (**e**), or PAG1 and TSN2 (**g**) in Col-0 and *pat2-2* mutant using PCC. **h** No significant difference in proteolytic activity is observed in supernatants or SG fractions between *pat2-2* mutant and Col-0 seedlings as revealed by the AMC release assays. **i**, **k** The *PAG1* knock-down mutants have no obvious effect on SGs disassembly (**i**), whereas SG disassembly is significantly delayed in *RPT2a/b* knock-down mutants (**k**). Scale bars: 10 μm. **j**, **l** Quantification of the percentage of cells with SGs in *PAG1* knock-down mutants (**j**) or *RPT2a/b* knock-down mutants (**k**). For **e**, **g**, **h**, **j** and **l**, data represent mean ± SD from three independent biological replicates. Statistical analysis in (**e**, **g**, **h**) was performed using a two-tailed unpaired Student's *t* test; in (**j**) and (**l**) was performed using one-way ANOVA with Tukey's multiple comparison test and different letters above the bars indicate statistical significance at $P < 0.05$. Confocal images were taken in the root meristem or transition zone of 5-day-old seedlings. Source data are provided as a Source Data file.

tagged AP-3β coprecipitated with MBP-tagged RPT2a but not PAG1 (Fig. 5c). These data collectively suggest that AP-3β interacts with the 19S RP subcomplex possibly via RPT2a/2b.

We next examined whether the 26S proteasome subunits participated in regulating SG dynamics. Both the RP subunits RPT2a and RPN1a, and the CP subunit PAG1 were recruited to SGs upon heat induction (Fig. 5d–g, Supplementary Fig. 10). We also investigated whether AP-3β regulated the sequestration of proteasome subunits to SGs. Notably, the RP subunits RPN1a and RPT2a significantly reduced their localization at SGs in *pat2-2* mutant upon heat induction. In contrast, the CP subunit PAG1 remained at SGs in this mutant (Fig. 5d–g, Supplementary Fig. 10), indicating that AP-3β selectively recruits the RP subunits to SGs upon heat induction.

Taken together, the biochemical and cell biology evidence suggests that AP-3β may serve as an adaptor to recruit the 19S RP subunits to SGs after heat stress.

The proteolytic activity of 20S proteasome is dispensable for SG disassembly in *Arabidopsis*

We next analyzed whether the sequestration of proteasome subunits to SGs is responsible for SG disassembly during heat recovery. According to the conventional theory, the 26S proteasome is mainly in charge of protein degradation. Therefore, we first tested whether the proteasome regulates SG disassembly through its proteolytic activity. However, cotreatment with the 20S proteasome inhibitors bortezomib (Btz) or MG-132 after heat stress had no obvious effects on SG disassembly (Supplementary Fig. 11a, b), although both chemicals inhibited the proteolytic activity of 20S CP to almost basal level (Supplementary Fig. 11c). Even more interestingly, no significant difference in proteolytic activity was observed in supernatants or SG fractions between *pat2-2* mutants and the control seedlings (Fig. 5h), although SG disassembly was significantly delayed in this mutant (Fig. 4d, e). Therefore, although the 26S proteasome subunits were recruited to SGs, SG disassembly may not be regulated through proteolytic activity of the proteasome in *Arabidopsis*.

To further corroborate the results, we generated estradiol-inducible artificial microRNA lines that specifically knocked down PAG1 (the core proteolytic subunit in CP) or RPT2a/b (RP subunits) respectively (Supplementary Fig. 12), as the null-mutants are lethal[39,40]. The PAG1 knock-down mutants exhibited strong growth defects, but SGs disassembled similarly to control seedlings after heat stress. In contrast, the knock-down mutants of RPT2a/b showed a significant delay in SG disassembly (Fig. 5i–l and Supplementary Fig. 12), suggesting that the RP subunits are crucial for SG disassembly during heat recovery. As AP-3β specifically interacts with the 19S RP subunits and is required for recruiting them to SGs, it may facilitate SG disassembly through non-proteolytic function of the proteasome via 19S RP.

The 19S RP-associated deubiquitylation is essential for SG disassembly

We next investigated the potential role of 19S RP in regulating SG disassembly. In yeast and mammalian cells, the non-proteolytic functions of RP have been reported, among which the RP-associated deubiquitylation regulates many biological processes[41–43]. Previous studies showed that three distinct family of deubiquitinases (DUBs)- RPN11, USP14, and UCH37 (also known as UCHL5)-are associated with the 19S RP of human proteasome[44,45]. Recently, cryo-EM structure of the 26S proteasome from *Spinacia oleracea* identified UBP6 (homolog of USP14 in human) and UCH2 (homolog of UCH37/UCHL5 in human) as proteasome-associated DUBs in plants[46]. To assess the potential role of DUBs on SG disassembly, we first employed the broad-spectrum DUBs inhibitor PR-619[47]. SG disassembly was almost abolished when cotreated with PR-619 during heat recovery (Supplementary Fig. 13), suggesting that the DUB activity is vital for SG disassembly. To further investigate which kind of DUBs regulates SG disassembly, we utilized selective inhibitors that specifically target one or a few DUBs[48–50]. Interestingly, co-treatment with b-AP15 or WP1130 (target RP-associated DUBs) significantly delayed SG disassembly, whereas capzimin (targets RP subunit RPN11) had no obvious effects. In addition, co-treatment with P22077 or TCID (target the proteasome-independent DUBs) did not affect SG disassembly (Fig. 6a, b, Supplementary Fig. 13). These data suggest that the RP-associated DUBs are important for SG disassembly during heat recovery. To further corroborate the conclusion, we generated transgenic lines that stably expressed UBP6-GFP or UCH2-GFP (RP-associated DUBs)[51,52]. Both UBP6 and UCH2 were sequestrated to SGs upon heat induction. In contrast, UBP12-GFP (proteasome-independent DUB) did not respond to heat stress and showed no obvious colocalization with the TSN2-labeled SGs (Supplementary Fig. 14a–c and 14f), although it plays important roles in many physiological processes[53], indicating that the RP-associated DUBs are preferentially recruited to SGs after heat induction. We also demonstrated that UBP6 and UCH2 interacted with the RP but not CP subunits before and after heat stress (Supplementary Fig. 14g–i), suggesting a close relationship between RP and DUBs.

We next assessed whether the SG components are regulated by DUBs. Upon heat induction, the SG fraction was highly enriched with ubiquitinated proteins, which rapidly reduced after heat release (Supplementary Fig. 15a), similar to recent publications in mammalian cells[9,11]. Cotreatment with the RP-associated DUBs inhibitor b-AP15 or WP1130 significantly delayed the deubiquitylation of SG components (Fig. 6c, d, Supplementary Fig. 15b, c). In contrast, the proteasome-independent DUBs inhibitor P22077 as well as the 20S CP inhibitor Btz showed no obvious effects on the deubiquitylation process (Supplementary Fig. 15d–g). Therefore, the RP-associated DUBs are responsible for the deubiquitylation of SG components during heat recovery.

Since deubiquitylation of SG components is not coupled with the proteolytic activity of the proteosome, we further investigated which lysine residue of ubiquitin (Ub) was modified for linkage in SG components. It was reported that K48-linked Ub chains are the primary signal for protein degradation via the proteasome[54]. Notably, only a small portion of SGs was recognized by the K48-linkage specific antibody (Fig. 6e), supporting the notion that the majority portion of SG components are not targeted for degradation by the proteasome. In contrast, the K63-linked ubiquitylated proteins were highly enriched in SGs after heat stress (Fig. 6e). Such K63-linked, but not K48-linked ubiquitylated proteins were also retained in SGs during heat recovery when cotreated with b-AP15 (Fig. 6f, g), indicating that the RP-associated DUBs preferentially target the K63-linked Ub chains for SG disassembly.

We next investigated whether AP-3β regulated the deubiquitylation process as well. Notably, the *pat2-2* mutants did not alter the abundance of ubiquitylated proteins in SGs upon heat stress; however, the deubiquitylation process was significantly delayed after heat release (Fig. 6h, i), indicating that AP-3β promotes the deubiquitylation of SG components during heat recovery. In line with this, the deubiquitinase activity in SG fraction was reduced in *pat2-2* mutants (Fig. 6j). We subsequently examined whether AP-3β regulates the sequestration of RP-associated DUBs to SGs. However, UBP6 and UCH2 were still recruited to SGs in *pat2-2* mutants (Supplementary Fig. 14d, e), indicating that AP-3β might indirectly regulate the deubiquitinase activity. It was reported that the RP-associated DUBs are self-inhibited; only upon binding to the 19S RP can their deubiquitinase activity be stimulated[51,55,56]. As AP-3β physically interacts with the RP subunits and is required for recruiting them to SGs, we further investigated whether AP-3β promotes deubiquitylation of SG components via the RP. Notably, the knockdown mutants of RPT2a/b but not PAG1, significantly slowed down the deubiquitylation of SG components during heat recovery (Supplementary Fig. 15h–k). The deubiquitinase activity in SGs was also significantly reduced in RPT2a/b knockdown mutants (Fig. 6k), suggesting that the 19S RP plays a crucial role in activating DUBs in SGs after heat stress.

https://doi.org/10.1038/s41467-025-57306-7

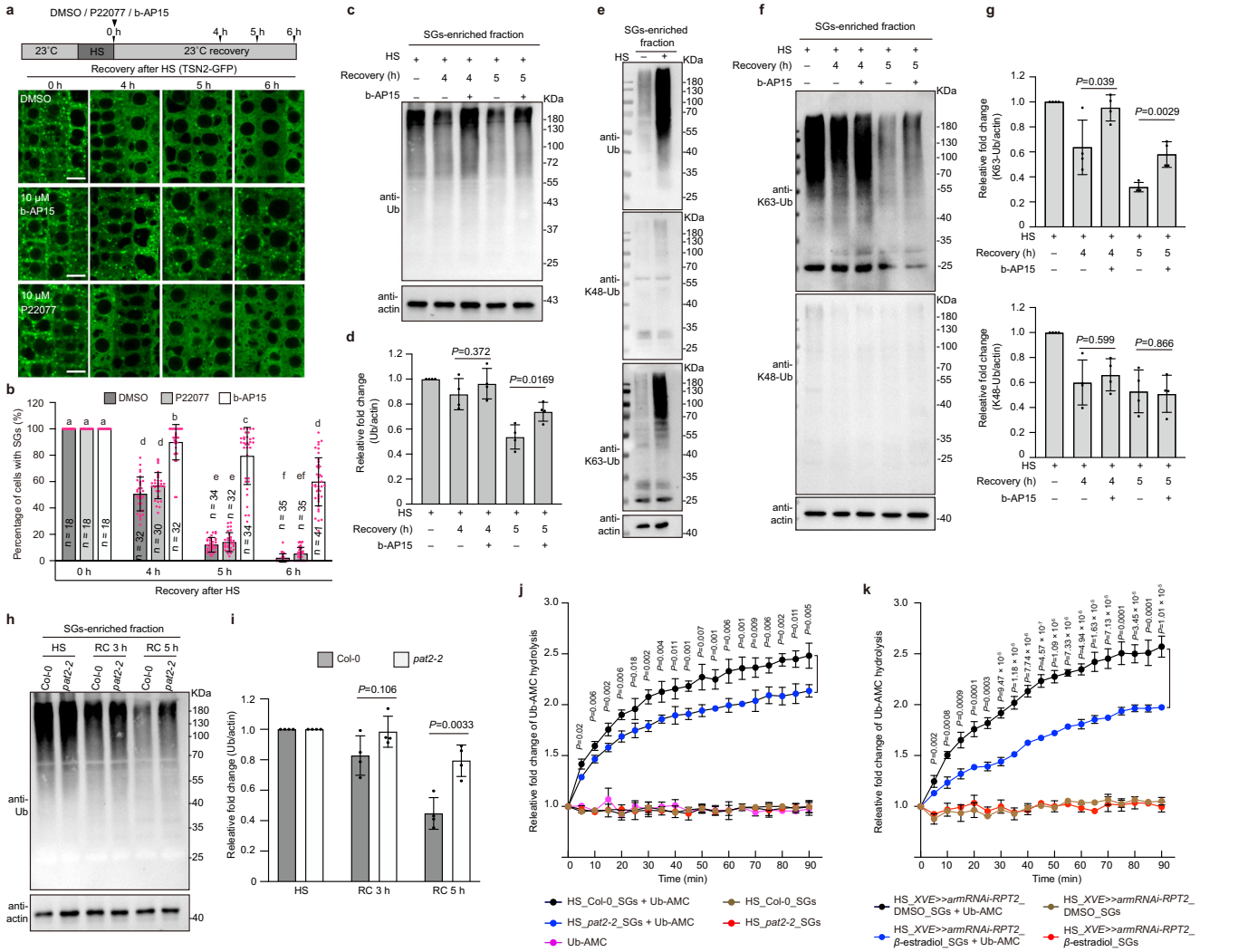

Fig. 6 | AP-3β regulates SGs disassembly via the 19S RP-associated deubiquitylation process during heat stress recovery. a Co-treatment with b-AP15 significantly delays SG disassembly, whereas P22077 has no obvious effects. Confocal images were taken in the root meristem or transition zone of 5-day-old seedlings. Scale bars: 10 μm. **b** Quantification of the percentage of cells with SGs as shown in (**a**). Data represent mean ± SD from three independent biological replicates. Statistical analysis was performed using one-way ANOVA with Tukey's multiple comparison test and different letters above the bars indicate statistical significance at $P < 0.05$. **c** Detection of the ubiquitinated proteins by immunoblot in SGs fractions with or without b-AP15 co-treatment during heat recovery. **d** Quantification of the relative fold changes of band intensity in (**c**). **e** Immunoblot analysis reveal that the K63-linked polyubiquitinated proteins are highly enriched in SGs fractions after heat stress whereas the K48-linked proteins are barely detected using the K48- or K63-linkage specific antibodies. **f** Detection of the K63-polyubiquitylated proteins by immunoblot in SG fractions with or without b-AP15 co-treatment during heat recovery. **g** Quantification of the relative fold changes of band intensity in (**f**). **h** Detection of the ubiquitylated proteins by immunoblot in SGs fractions from Col-0 seedlings or *pat2-2* mutants during heat recovery. **i** Quantification of the relative fold changes of band intensity in (**h**). **j** Ub-AMC hydrolysis assays show the deubiquitinase activities in heat-induced SGs is significantly reduced in *pat2-2* mutant compared to Col-0 seedlings. **k** Ub-AMC hydrolysis assays show the deubiquitinase activities in heat-induced SGs is significantly reduced in *RPT2* knock-down mutant after estradiol induction. For **c**, **e**, **f** and **h**, the anti-actin antibody was utilized as a loading control in parallel. For **d**, **g** and **i**, data represent mean ± SD from four independent biological replicates. For **j** and **k**, data represent mean ± SD from three independent biological replicates. For **d**, **g**, **i**, **j** and **k**, statistical analysis was performed using a two-tailed unpaired Student's *t* test. Source data are provided as a Source Data file.

As AP-3β physically interacts with TSN1/2, we further analyzed whether the TSN proteins also regulate the DUBs. For this purpose, we co-expressed the *UBP6-GFP* and *RFP-RBP47b* constructs using protoplasts isolated from Col-0 seedlings or *tsn1tsn2* mutants. The sequestration of UBP6 to SGs was significantly reduced in protoplasts from *tsn1tsn2* mutants compared to those from Col-0 seedlings (Supplementary Fig. 15l, m). Consistent with this, the DUB activity was dramatically reduced in *tsn1tsn2* mutants (Supplementary Fig. 15n). Therefore, the TSN1/2-AP-3β module is crucial for maintaining the proper function of DUBs in SGs.

These data collectively support that AP-3β promotes deubiquitylation of SG components, which is essential for SG disassembly following heat release.

The deubiquitylation targets downstream of AP-3β primes plants for translation reinitiation and growth recovery

We continued our analysis to identify deubiquitylation targets downstream of AP-3β during heat recovery. Due to detection limitations, we could not use AP-3β or TSN2-immunoprecipitated SG samples for ubiquitinome analysis. Instead, we isolated SG-enriched fractions from

https://doi.org/10.1038/s41467-025-57306-7

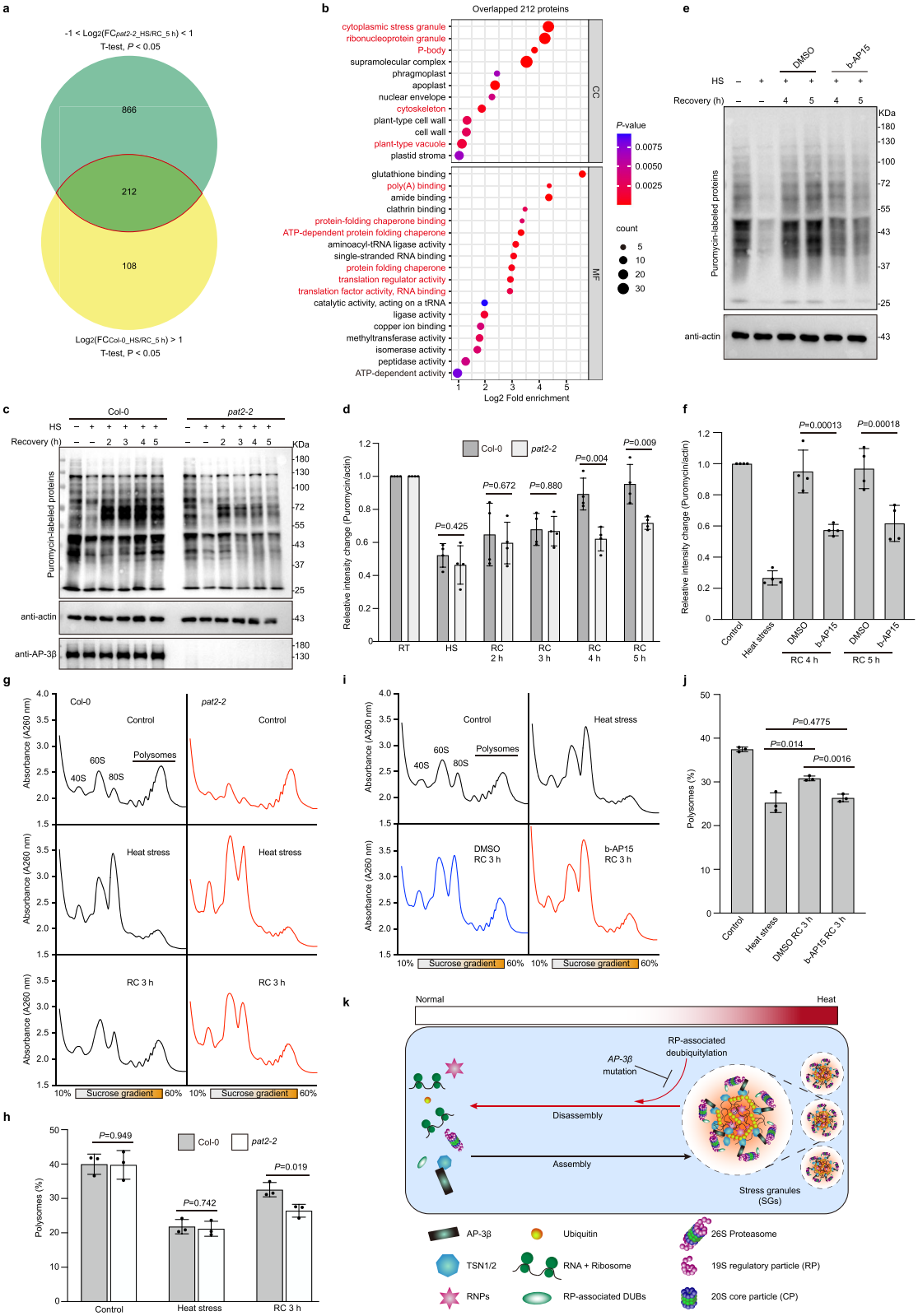

Col-0 seedlings or *pat2-2* mutants after heat stress (0 h) and at 5 h after heat recovery, and conducted quantitative ubiquitinome analysis. The target proteins may include SG core proteins and SG shell proteins that are easily excluded during IP step, as well as non-SG components. Quantitative analysis revealed that compared to Col-0, ubiquitylated proteins that were preferentially enriched in SG fractions of *pat2-2* mutants at 5 h after heat recovery [$Log_2(FC_{Col\text{-}0\_HS/RC\_5\ h})$ >1 and −1 <$Log_2(FC_{pat2\text{-}2\_HS/RC\_5\ h})$ <1; T-test, $P < 0.05$] can be categorized into cytoplasmic stress granules, ribonucleoprotein (RNP) granules, protein folding chaperones, translation factors, cytoskeleton, and plant-type vacuole (Fig. 7a, b and Supplementary Data S4). Of these proteins, 22.6% of these proteins overlapped with the SG components identified by immunoprecipitation coupled with mass spectrometry (IP-mass) in previous studies[14,20] (Supplementary Fig. 16a and Supplementary

Fig. 7 | The deubiquitylation targets downstream of AP−3β primes plants for translation reinitiation and growth recovery. a Venn diagram reveals the ubiquitylated proteins that are preferentially enriched in SG fractions of *pat2-2* mutants compared to Col-0 seedlings during recovery after heat stress [$Log_2(FC_{Col\text{-}0\_HS/RC\_5\ h})$ >1 and −1 <$Log_2(FC_{pat2\text{-}2\_HS/RC\_5\ h})$ <1; T-test, $P < 0.05$]. Statistical analysis was performed using a two-tailed unpaired Student's *t* test. **b** The enriched cellular components (CC) and molecular functions (MF) GO terms of overlapped proteins as shown in (**a**). The translation reinitiation efficiency is significantly reduced in *pat2-2* mutant (**c**) or after b-AP15 treatment (**e**) during heat recovery, as revealed by surface sensing of translation (SUnSET) assays. Immunoblot with an anti-puromycin antibody was utilized to assess the translation status. The anti-actin antibody was used as a loading control in parallel. **d**, **f** The relative fold change of band intensity in (**c, e**) was quantified. Translation reinitiation efficiency is significantly reduced in *pat2-2* mutant (**g**) or after b-AP15 treatment (**i**) during recovery after heat stress, as revealed by polysome profiling. **h**, **j** Quantification of the percentage of polysome/total fractions under different conditions as shown in (**g**, **i**). **k** Proposed model for SGs disassembly during heat recovery. Heat induces rapid assembly of SGs, which are composed by RNAs, RNA-binding proteins (RBPs), proteasome subunits, RP-associated deubiquitinases (DUBs), and some endomembrane proteins such as AP-3β. The RP-associated deubiquitylation process is crucial for SGs disassembly and translation reinitiation after heat release. Mutation in AP-3β impairs the recruitment of RP subunits to SGs, resulting in delayed SGs disassembly and reduced growth recovery. For **d**, **f**, **h**, **j**, data represent mean ± SD from at least three independent biological replicates and statistical analysis was performed using a two-tailed unpaired Student's *t* test. Source data are provided as a Source Data file.

Data S2). Interestingly, most of the overlapped proteins are translation regulators and RBPs. Therefore, we next further investigated whether AP-3β promoted SG disassembly via translation regulation. Puromycin binding is commonly used to monitor the translation status and newly synthesized proteins[57,58]. In control plants, heat stress led to a significant decrease in puromycin binding abundance, which gradually increased during stress recovery (Fig. 7c, d). The *pat2-2* mutants exhibited similar puromycin binding abundance before heat stress and upon heat induction. However, the restoration of puromycin binding was significantly delayed in the mutant during heat recovery, indicating impaired resumption of translation (Fig. 7c, d). Such delay in translation reinitiation was also observed when cotreated with the RP-associated DUBs inhibitor b-AP15 or WP1130, but not with the RP-independent DUBs inhibitor capzimin or P22077 (Fig. 7e, f, Supplementary Fig. 17). Moreover, the defects in translation reinitiation were further confirmed by polysome profiling, with the ratio of polysome fraction significantly reduced in *pat2-2* mutants and after b-AP15 treatment during heat recovery (Fig. 7g–j). These findings collectively underscore the importance of AP-3β and RP-associated DUBs on translation reinitiation after heat stress release.

In addition, we also identified a set of vacuolar transport components as the deubiquitylation targets downstream of AP-3β (Supplementary Fig. 16b, c and Supplementary Data S2) that are not reported in other publications. This may due to method differences (without IP step), or because our sample include some non-SG components. Therefore, we further investigated whether vesicle transport plays a role in SG disassembly. Brefeldin A (BFA) is a widely used inhibitor that blocks the ER-to-Golgi transport[59,60] while wortmannin (WM) is a phosphatidylinositol 3-kinase (PI3K) inhibitor that induces MVB to swell and disrupts autophagosome biogenesis[61,62]. Interestingly, wortmannin but not BFA treatment could efficiently inhibit SG disassembly (Supplementary Fig. 16d, e). Given that autophagy is dispensable for SG disassembly after heat release (Supplementary Fig. 9), the deubiquitylation process downstream of AP-3β may target proteins involved in MVB dynamics. Notably, one of the targets, SKD1, a subunit of the endosomal complex required for transport (ESCRT) essential for MVB biogenesis[63], was recently reported to translocate to SGs and interact with the SG core RBPs after heat stress[64], suggesting that the proper function of MVBs might be important for SG dynamics. As MVBs in plant cells are recognized as the pre-vacuolar compartments (PVCs)[65], it is plausible to speculate that vacuolar transport might play a role in regulating SG disassembly.

Overall, our data suggest that the deubiquitylation downstream of AP-3β targets RBPs and vacuolar transport components. The two sets of proteins may act synergistically to promote SG disassembly and plant growth recovery.

Discussion

SGs are highly dynamic and reversible membraneless compartments that assemble in the cytoplasm in response to environmental stresses. They serve as a protective storage site for messenger RNAs, shielding them from stress-induced degradation[5,66]. Persistent SGs or dysregulation of SG disassembly can have detrimental effects on cell adaptation and survival after stress remission[2,66,67]. Therefore, understanding the mechanism for SG disassembly has become an important research focus in recent years. In this study, we have uncovered an important role of the 19S RP in promoting SG disassembly. The 19S RP-associated deubiquitylation is crucial for SG disassembly and translation reinitiation after heat release. Mutation in AP-3β impairs the recruitment of RP subunits to SGs and reduces DUB activity, resulting in delayed SG disassembly and compromised plant growth recovery. The major findings of our research are summarized in a model shown in Fig. 7k.

Endomembrane system is important for supporting RNA granule dynamics in plant cells

For a long time, membrane system and membraneless condensates are considered to work independently. Yet, recent studies are uncovering the close interactions between these two systems[68,69]. In this study, while initially investigating the interaction proteins of AP-3β, we unexpectedly discovered its unconventional role in promoting SG disassembly through interaction with TSN1/2. In addition, we found that AP-3β colocalizes with TSN2 at the PM, and the AP-3β- and TNS2-positive SGs do not recover after photobleach. In contrast, the RBP47b-labeled SGs behave like liquid and rapidly recover (Supplementary Fig. 5). This suggests the coexistence of two populations of SGs in plant cells: the membrane-associated and liquid-like SGs. Interestingly, not only AP-3β itself belongs to endomembrane system but also the deubiquitylation targets downstream of AP-3β include vacuolar transport components (Supplementary Fig. 16c). For AP-3β, its sequestration in SGs after heat stress as well as its function in growth recovery requires its membrane-association property (Figs. 3 and 4). The impediment of SG disassembly was observed in *pat2-2* mutants and after wortmannin treatment (Fig. 4d, e and Supplementary Fig. 16d, e). All these evidences imply that endomembrane proteins are not passively recruited to SGs but actively participate in regulating SG dynamics.

Given that AP-3β physically interacts with TSN1/2 and the 19S RP subunits before heat induction, these three sets of proteins may preassemble into a large complex before SG assembly. As TSN1/2 act as the nucleation platform for SGs through interaction with RNAs and RBPs[13,27], such a preassembled complex, along with its membrane-association characteristics, may alter the biophysical property of SGs. This could ultimately change the SG disassembly kinetics and the fate of residing RNAs.

Recent studies have also shed light on the association of PBs with endomembrane system. DECAPPING PROTEIN 1 (DCP1), a consistent component of PBs, is localized to specific PM subdomains via its interaction with the actin-nucleating SCAR–WAVE complex[70]. This SCAR/WAVE-DCP1 regulatory module determines the size of PBs and mRNA turnover rate[71]. Interestingly, AP-3β also colocalizes with TSN2 at the PM (Supplementary Fig. 5a–c), and the deubiquitylation targets downstream of AP-3β include cytoskeleton regulators (Fig. 7b,

Supplementary Data 2). The membrane-associated TSN1/2 proteins can restrict the exchange rate of RBP47b between SGs and the cytoplasm[13]. Thus, the endomembrane-cytoskeleton network may modulate the balance between SGs and PBs, as well as the corresponding mRNA fate.

A unique function of 19S RP in disassembling heat-induced SGs in plants

Over the past decade, autophagy and ubiquitin-proteasome system (UPS) have been reported to promote SG disassembly in yeast and mammalian cells[6,8,9,11]. In this project, we have demonstrated that autophagy is dispensable for SG disassembly during heat recovery in *Arabidopsis* (Supplementary Fig. 9). While both 20S CP and 19S RP subunits are recruited to SGs after heat stress, inhibiting the proteolytic activity of the CP either by inhibitors (Btz and MG132) or genetic knock-down of the CP core subunit has no adverse effect on SG disassembly (Fig. 5i, j and Supplementary Fig. 11). In contrast, SG disassembly is significantly impeded in *pat2-2* mutants and knockdown mutants of RP subunits (Figs. 4d, e and 5k, l). The non-proteolytic functions of RP have been revealed in many biological processes, including the transcription initiation and elongation[72,73], mRNA export[74], ubiquitin-dependent histone modification[75], and heterochromatin regulation[76]. A recent study by Sun et al reported the presence of excessive free RP subcomplexes in neurons, acting as independent DUBs to deubiquitylate synaptic proteins essential for synaptic vesicle release[77]. Although we don't know whether free RPs also exist in heat-induced SGs in plant cells at current stage, these SG-enriched RPs are crucial for DUB activity, thus may function similarly to the RPs in neurons. Alternatively, the 19S RP may act as a large chaperon to remodel the misfolded SG components. The base complex of RP contains six ATPases subunits with chaperon activity[78], and the 19S RP has been reported to regulate heterochromatin spreading and assist transcription activation through its chaperon activity[76]. More detailed understanding of the unique function of RP would require structural information about the proteasome in plants, particularly under stress conditions.

Who perceives the ubiquitin signals in SGs? Different effectors in different experimental systems

While SG assembly is driven by liquid-liquid phase separation, SG disassembly is not a simple reverse process. The disassembly of SGs occurs concurrently with the release of stored mRNA and translation reinitiation. Studies from mammalian cells have elucidated that ubiquitin is a prominent PTM signal disposed on SG components[9,12]. Such enrichment of ubiquitylated proteins in SGs is also observed in our results in *Arabidopsis*, indicating that this might be a universal phenomenon among different eukaryotic systems. Interestingly, both our data (Fig. 6e) and several published works[9,12,38] in mammalian cells suggest that K63-polyubiquitin is the major ubiquitin signal in SG components. As a common knowledge, K63-conjugated proteins cannot be directly targeted by the 26S proteasome for degradation[79]. Yet, different experimental systems reveal different effectors that can recognize the signals. Gwon et al. reported that in U2OS cells, the SG core RBPs are K63-ubiquitylated upon heat induction, which are targeted by the ER-associated segregase p97/Cdc48/VCP after heat release. p97/Cdc48/VCP extracts RBPs from SGs to promote SG disassembly and translation reinitiation[11]. Pan et al. reported that a majority portion of SG components are subjected to K63-linked polyubiquitylation under oxidative stress in HEK293 cells, which are targeted by the autophagy-related pathway for SG clearance[12]. In our work, although K63-conjugated ubiquitylated proteins are highly enriched in SGs from heat-stressed Arabidopsis seedlings, neither autophagy nor 20S CP promote the disassembly of heat-induced SGs. In contrast, the 19S RP-associated deubiquitinases are the key determinants for SG disassembly. Therefore, different effectors are employed to perceive the ubiquitin signals for subsequent processes to promote SG disassembly.

A recent publication by Xie et al.[20] revealed that the proteolytic activity of 20S proteasome is important for disassembling the RBP47b-labeled SGs after heat stress. We believe that our different conclusions arise from several aspects. Firstly, they employed RBP47b as the major SG marker, which we have shown to display different mobility compared to TSN2. However, the *rbp47abcc'* quadruple mutants do not affect SG induction[20]. In contrast, the *tsn1tsn2* double mutants significantly reduce the size and number of SGs after heat stress[13,27], suggesting that the membrane-associated TSN1/2 are the primary scaffold proteins for the heat-induced SGs. Therefore, their behavior post-heat release likely reflects the real situation in vivo. Secondly, we evaluated SGs in different root regions. While they focused on the root elongation zone, we assessed the SG dynamics in the root meristem and transition zone. Thirdly, we used different heat treatment methods. They used incubator for the heat treatment, while we utilized water bath to heat the entire medium plate containing seedlings. The water bath method results in stronger heat stress, necessitating a longer recovery period. Fourthly, we employed different drugs and detection methods. They utilized MG132 as the sole 20S CP inhibitor, while we used Btz or MG132. Btz is recognized as a more specific inhibitor of 20S CP whereas MG132 is known to induce apoptosis[80,81]. Over half of their data quantified the SG dynamics and analyzed the ubiquitin abundancy in SGs by cotreating with MG132 alongside heat induction, whereas we only applied MG132 or Btz after heat release. In our study, we captured SG images at different time points during heat recovery without fixation, whereas they used a FISH buffer that contains 50% heptane and 10% DMSO for fixation. High concentration of DMSO is known to induce membrane perforation[82,83], which could be more pronounced after heat treatment.

Nonetheless, the K63-conjugated ubiquitylated proteins are highly enriched in heat-induced SGs from Col-0 non-transgenic plants without drug treatment (Fig. 6e). This indicates that the majority of SG components are not targeted by 20S proteosome for proteolysis, regardless of the SG marker used, fixation methods, or detection area. However, we cannot exclude the possibility that a small portion of SG components can still be targeted for degradation via the proteasome. K63-polyubiquitination is recognized as a regulatory signal. Recent studies suggest that K63-polyubiquitination targets the ribosomal subunits and initiation factors for translation control through structural changes under stress conditions[84,85]. Given that RP-associated DUBs specifically target the K63 ubiquitin-modified SG components, they may regulate the translation machinery via signaling functions. In plant cells, K63-polyubiquitination also serves as a tag for protein degradation by the vacuolar transport pathway[86]. Although 20S CP and autophagy is dispensable for disassembling the heat-induced SGs, wortmannin treatment obviously inhibits SG disassembly (Supplementary Fig. 16d, e). As wortmannin inhibits the MVB-to-vacuole transport by disrupting MVB function, vacuolar transport might play a role in regulating SG disassembly through the degradation of SG components. This combination of translation control and MVB-based vacuolar transport machinery can enable plants to rapidly restore growth after stress release, which is essential for plant survival under adverse conditions. Further studies on the specific targets of RP-associated DUBs and their functional consequences will provide valuable insights into the intricate regulation of stress adaptation in plants.

Methods

Plant materials and growth conditions

Arabidopsis thaliana ecotype Columbia (Col-0) was utilized as wild type in this study. Stable transgenic lines of *ProAP-3β::AP-3β-GFP*[25], *ProVAMP721::mRFP-VAMP721*[87], *ProUBQ::mCherry-SYP32*[30], *ProTSN1::TSN1-GFP*[13], *ProTSN2::TSN2-GFP*[13], *Pro35S::GFP-RBP47b*[14], *Pro35S::PAB2-RFP*[88], *Pro35S::mCherry-DCP5*[89], *ProRPN1a::RPN1a-GFP*[90] and T-DNA insertion

mutants of *pat2-2* (SAIL_1258_G03)[25], *pat4-2* (SALK_069881)[24], *dcp5-1* (SALK_008881)[89] and *tsn1tsn2* double mutant[13] in the Landsberg *erecta* (Ler) and Col-0 backgrounds were described previously. The following T-DNA insertion mutants of *ap-3μ-3* (SALK_127431), *tsn2* (SALK_052200), *hsp101* (SALK_099583), *atg7-2* (GK-655B06) were obtained from the Arabidopsis Biological Resource Center (ABRC) or Nottingham Arabidopsis Stock Centre (NASC).

Seeds were surface sterilized using a 0.25% sodium hypochlorite solution, followed by four washes with sterile water. The sterilized seeds were then stratified in darkness at 4 °C for two days. For confocal observation or protein extraction, the stratified seeds were germinated and grown vertically on square plates containing half-strength Murashige & Skoog (MS, PhytoTech, M524) medium (pH 5.6) with 1% (w/v) sucrose and 0.8% (w/v) Phytoagar in a growth chamber (Percival CU-36L) at 22 °C under a long-day photoperiod (16 h light/8 h dark) for the indicated time.

Plasmid construction and generation of the transgenic plants

The amplified fragments of *GFP-T35S* or *RFP-T35S*, derived from pUBC-GFP-Dest and pUBC-RFP-Dest[91] vectors, were subcloned into *SpeI*- and *XbaI*-digested pH7GWR2 vector to generate the pH7_*Pro35S::GFP* and pH7_*Pro35S::RFP* vectors utilized in this paper. To create the constructs of *ProAP-3β::AP-3β-GFP*, *ProRPT2a::RPT2a-GFP* and *ProTSN2::TSN2-RFP*, genomic DNA (gDNA) fragments of *AP-3β*, *RPT2a* and the coding sequence of *TSN2*, were cloned from wild-type gDNA or cDNA, and assembled into *SpeI*-digested pH7_*Pro35S::GFP* or pH7_*Pro35S::RFP* vectors. Subsequently, the 35S promoter fragment in each constructs were double-digested by *SalI* and replaced with an approximately 2 kb native promoter fragments of *AP-3β*, *RPT2a* or *TSN2*. To generate the constructs of *ProAP-3β::AP-3βΔIDR-GFP* and *ProAP-3β::AP-3βΔAP3β_C-GFP*, the *ProAP-3β::AP-3β-GFP* vector was double-digested with *SpeI*, and the truncated gDNA fragments lacking the *IDR* region or *AP3β_C* domain were amplified and assembled into *SpeI*-digested *ProAP-3β::AP-3β-GFP* vector. For the constructs of *ProAP-3β::AP-3βΔN-GFP* and *ProPAG1:PAG1-GFP*, approximately 2 kb native promoters of *AP-3β* or *PAG1*, along with the corresponding gDNA fragments of *AP-3βΔN* or *PAG1*, were amplified and subcloned into *HindIII*- and *SpeI*-digested pH7_*Pro35S::GFP* vector. To generate the constructs of *Pro35S::RFP-RBP47b* and *Pro35S::RFP-ATG8e*, the coding sequences of RBP47b and ATG8e were amplified from cDNA and introduced into pDONR207 via BP reaction, followed by LR reaction to the destination vector pH7GWR2. The *ProUBQ::UBP6-GFP* construct was generated by assembling the coding sequence of *UBP6* into *BamHI*-digested pCAMBIA1300-UBQ-GFP vector. To create the *ProUBQ::UBP12-GFP-FLAG* construct, the GFP fragment was first assembled into the *SmaI*-digested *pCAMBIA1300-35S-UBP12-FLAG* vector[92], followed by digestion with *SbfI* and *XbaI* to replace the *35S* promoter with *UBQ* fragment. The *ProUBQ::UCH2-GFP-FLAG* construct was generated by assembling the fragments of *UBQ* promoter and *UCH2* coding sequence into *SalI*-digested *ProUBQ::UBP12-GFP-FLAG* vector.

All constructs were introduced into Col-0 or mutant plants via Agrobacterium (*Agrobacterium tumefaciens*, strain GV3101)-mediated transformation using the standard floral dipping method. Positive transgenic seedlings were selected on 1/2 MS plates supplemented with 100 mg/ml cefotaxime and either 30 mg/ml hygromycin, 30 mg/ml basta or 50 mg/ml kanamycin. Homozygous transgenic lines were used for subsequent experiments.

Luciferase complementation imaging (LCI) and bimolecular fluorescence complementation (BiFC) assays

LCI assays were conducted as previously described[31]. The coding sequences of *AP-3β*, *AP-3δ*, *VPS41*, *AP-3β_N*, *AP-3β_C*, *AP-3βΔIDR* and *AP-3βΔAP3β_C* were cloned into *KpnI*- and *SalI*-double digested pCAMBIA1300-35SC-Nluc vector to produce the constructs of AP-3β-Nluc, VPS41-Nluc, AP-3β_N-Nluc, AP-3β_C-Nluc, AP-3βΔIDR-Nluc and AP-3βΔAP3β_C-Nluc. Similarly, the coding sequences of *AP-3δ*, *TSN1*, *TSN2* and *PAB2* were cloned into *KpnI*- and *SalI*-double digested pCAMBIA1300-35SN-Cluc vector to produce the constructs of Cluc-AP-3δ, Cluc-TSN1, Cluc-TSN2 and Cluc-PAB2.

For BiFC assays, the *attR1-attR2* fragments from the pUBQ10-DEST vector[91] and *HA-T35S* or *Myc-T35S* from the rBiFC-2in1-CC vector[93] were amplified and cloned into *SpeI*- and *XbaI*-double digested pB7WGR2 vector to generate the destination vectors pB7WG_YN and pB7WG_YC. The coding sequences of *AP-3β*, *VPS41*, *AP-3β_N*, *AP-3β_C*, *AP-3βΔIDR* and *AP-3βΔAP3β_C* were cloned into *SpeI*-digested pB7WG_YN vector to produce the constructs of AP-3β-YN, AP-3δ-YN, VPS41-YN, AP-3β_N-YN, AP-3β_C-YN, AP-3βΔIDR-YN and AP-3βΔAP3β_C-YN. Similarly, the coding sequences of *AP-3δ*, *TSN1*, *TSN2* and *PAB2* were cloned into *SpeI*-digested pB7WG_YC vector to produce the constructs of AP-3δ-YC, TSN1-YC, TSN2-YC and PAB2-YC.

All constructs described above were transformed into *Agrobacterium* strain GV3101 and infiltrated into *N. benthamiana* leaves, following previously established protocols[31].

Yeast two-hybrid assay

The coding sequences of AP-3β, RPN1a, RPN5a, RPN12a, RPT1a, RPT2a, RPT2b, AP-3δ, PAC1, PBF1, PAG1 and PAD1 were amplified and cloned into the pGBKT7 or pGADT7 vectors. Sequence-verified clones were co-transformed into the yeast strain AH109. The co-transformed yeast clones were initially selected on SD medium lacking leucine (Leu) and tryptophan (Trp). The selected colonies were subsequently transferred to SD medium lacking histidine (His), leucine (Leu), and tryptophan (Trp) for interaction tests.

Antibodies production

To produce the anti-TSN1/2, anti-AP-3β and anti-AP-3δ antibodies, fragments of coding sequences encoding amino acids (aa) 770-985 of TSN2, 650-900 aa of AP-3β and 639–869 aa of AP-3δ were subcloned into the pGEX4T-AB1 vector. These re-constructed vectors were sent to ABclonal company (Wuhan, China) for immunization and antibody purification. Two rabbits were immunized. The antibodies were affinity-purified using HiTrap Columns coupled with antigens.

Protein expression, purification and in vitro pull-down analysis

To express and purify proteins, the coding sequences of *TSN1*, *TSN2*, *AP-3β*, *AP–3β_N, AP-3β_C, RPT2a* and *PAG1* were cloned into the *EcoRI*-digested pMAL-c2x vector or pGEX-4T-1 vectors. This resulted in the production of fusion proteins: MBP-TSN1, MBP-TSN2, MBP-AP-3β_N, MBP-AP-3β_C, MBP-RPT2a, MBP-PAG1, GST-AP-3β, and GST-TSN2. Recombinant proteins were induced in Escherichia coli strain BL21(DE3) with 0.5 mM IPTG and incubated overnight at 16 °C. Following centrifugation, the cells were lysed, and the recombinant proteins were purified with the GST-Sefinose(TM) resin 4FF (Sangon; C600031), Ni-IDA-Sefinose(TM) resin 6FF (Sangon; C600029) or amylose resin (New England Biolabs; E8021S) according to the manufacturer's instructions. The purified proteins were stored at −80 °C with 10% glycerol until further use.

To perform pull-down assay, 4 μg of recombinant proteins, including MBP-TSN1, MBP-TSN2, MBP-AP-3β_N, MBP-AP-3β_C, MBP-RPT2a or MBP-PAG1 were incubated with either GST, GST-AP-3β or GST-TSN2 in 1 mL of pull-down buffer [50 mM Tris-HCl (pH 7.5), 150 mM NaCl, 1 mM EDTA, 1% (v/v) glycerol, 0.2% (v/v) Triton-X 100] at 4 °C for 2 h with gentle rotation. Following incubation, the proteins were pulled down with GST resin for 1 h. Subsequently, the proteins were analyzed using immunoblotting with a GST antibody (Abbkine; A02030, 1:5000) or an MBP antibody (New England Biolabs; E8032S, 1:10000). HRP-conjugated goat anti-mouse secondary antibody (Sangon; D110087, 1:10000) was utilized for detection.

LC-MS/MS for AP-3β-GFP immunoprecipitation

For immunoprecipitation followed by mass spectrometry (IP-MS), protein extraction was conducted as previously described[31]. 7-day-old

transgenic seedlings expressing *ProAP-3β::AP-3β-GFP* and *ProUBQ::GFP* were ground in a pre-chilled mortar and pestle on ice using extraction buffer [150 mM Na-HEPES, pH 7.5, 10 mM EDTA, 10 mM EGTA, 17.5%(w/v) sucrose, 7.5 mM KCl, 0.01%(v/v) Igepal CA-630, 10 mM dithiothreitol, 1% (v/v) protease inhibitors (Roche; 11836170001)], with 2 mL buffer per 1 g of tissue (fresh weight). The homogenate was then filtered through two layers of Miracloth (Millipore, 475855-1R), and the flow-through was centrifuged at 4 °C, 6000 × *g* for 15 min. The supernatant was then divided into two replicate samples. For the IP-MS assay, 20 µL GFP-Trap Sepharose beads (ChromoTek; gta-20) were added to the supernatant and gently rotated at 4 °C for 6 h. The slurry was washed five times with pre-chilled extraction buffer (without protease inhibitors). Proteins were eluted using 30 µL 1× NuPAGE™ LDS sample buffer (Thermo; NP0007) by boiling at 90 °C for 10 min for subsequent liquid chromatography-tandem MS (LC-MS/MS) analysis.

The LC–MS/MS assay was conducted by Protein World Biotech (Beijing, China). Following immunoprecipitation, each gel band containing eluted proteins underwent reduction with 10 mM DTT for 30 min at 60 °C, alkylation with 20 mM iodoacetamide for 45 min at room temperature in the dark, and digestion with trypsin (sequencing grade, Thermo Scientific Cat#90058), The samples were then incubated overnight at 37 °C. Peptides were extracted twice with 5% formic acid, 60% acetonitrile and dried under vacuum. Samples were analyzed using Nano LC-MS/MS (Dionex Ultimate 3000 RLSCnano System, Thermofisher) interfaced with Eclipse (Thermofisher). The samples were loaded on to a fused silica trap column Acclaim PepMap 100, 75 µm × 2 cm (ThermoFisher). After washing with 0.1% TFA at 5 µl/min for 5 min, the trap column was brought in-line with an analytical column (Nanoease MZ peptide BEH C18, 130 A, 1.7 µm, 75 µm × 250 mm, Waters) for LC-MS/MS. Peptides were fractionated at 300 nL/min using a segmented linear gradient 4-15% B in 30 min (where A: 0.2% formic acid, and B: 0.16% formic acid, 80% acetonitrile), 15–25%B in 40 min, 25–50%B in 44 min, and 50–90%B in 11 min. Solution B then returns at 4% for 5 min for the next run.

The scan sequence began with an MS1 spectrum (Orbitrap analysis, resolution 120,000, scan range from M/Z 375–1500, automatic gain control (AGC) target 1E6, maximum injection time 100 ms). The top S (3 s) duty cycle scheme were used for determine number of MSMS performed for each cycle. Parent ions of charge 2–7 were selected for MS/MS and dynamic exclusion of 60 s was used to avoid repeat sampling. Parent masses were isolated in the quadrupole with an isolation window of 1.2 m/z, automatic gain control (AGC) target 1E5, and fragmented with higher-energy collisional dissociation with a normalized collision energy of 30%. The fragments were scanned in Orbitrap with resolution of 15,000. The MS/MS scan ranges were determined by the charge state of the parent ion but lower limit was set at 110 amu.

Mass spectrometry data analysis

Raw mass spectrometry (MS) data from co-immunoprecipitation (co-IP) experiments were searched against a database composed of Arabidopsis protein fasta database (Araport11) and processed using MaxQuant software (V1.6.7) to perform protein and peptide identification (FDR < 0.01), peak extraction and label-free quantification. Processed data were imported into Perseus (V2.0.11) (https://www.maxquant.org/perseus/) for downstream statistical analysis by standard procedure, including contaminants filtering, LFQ intensity Log_2 transformation, grouping of samples, missing value imputation, and identification of significant protein enrichments. Volcano plots were generated using Perseus to visualize differential protein expression and identify potential protein-protein interactions based on fold-change (≥2) and statistical significance (two-tailed unpaired Student's *t* test, $P < 0.05$).

Chemical stocks

Stock solutions of 50 mM cycloheximide (CHX, Selleck, S7418), 4 mM FM4-64 (Invitrogen, F34653), 50 mM MG-132 (Solarbio, IM0310), 10 mM Bortezomib (Beyotime, SC0263), 10 mM PR-619 (APExBIO, A8212), 20 mM capzimin (MedChemExpress, HY-110404), 10 mM b-AP15 (Beyotime, SG0020), 10 mM WP1130 (MedChemExpress, HY-13264), 10 mM P22077 (MedChemExpress, HY-13865), 10 mM TCID (MedChemExpress, HY-18638), 60 mM puromycin (MedChemExpress, HY-B1743A), 50 mM BFA (MedChemExpress, HY-16592), 35 mM Wortmannin (APExBIO, A8544) and 5 mM estradiol (Sigma-Aldrich, E2758) were prepared by dissolving them in DMSO. All chemicals were applied at 1:1000 dilution of the stock solutions.

Chemical treatments and confocal microscopy

For the induction of SGs, transgenic seedlings expressing GFP, mCherry or RFP fusion proteins were germinated and grown on 1/2 MS solid medium for 5 days. Heat stress was conducted using a water bath at 39 °C for 40 min. For CHX treatment, 5-day-old seedlings were transferred to 1/2 MS solid medium containing 35 µM CHX and incubated at room temperature for 1 h, followed by heat treatment at 39 °C for 40 min. To test the effects of chemicals on SG disassembly, heat-stressed seedlings were transferred to 1/2 MS liquid medium supplemented with DMSO or the respective chemicals. Confocal images were captured in root meristem or transition zone at specified time points during recovery.

Microscopy images were acquired using a Zeiss LSM880 confocal microscope with a ×40/1.2 water objective or Leica SP8 confocal microscope with a 63×/1.2 water objective. GFP was excited at 488 nm, and the emission signals were detected at 500–545 nm. YFP was excited at 514 nm, and the emission signals were detected at 520–545 nm. RFP, mCherry and FM4-64 were excited at 552 nm, and the emission signals were detected at 570–620 nm.

Fluorescence recovery after photobleaching (FRAP) assay

5-day-old transgenic seedlings of *ProAP-3β::AP-3β-GFP*, *ProTSN2::TSN2-GFP* and *Pro35S::GFP-RBP47b*, grown on 1/2MS solid medium in a petri dish, were subjected to heat stress for 40 min before FRAP analysis. The FRAP mode of Leica SP8 software was set up for the acquisition of one prebleach image, one bleach scan, and 20 postbleach scans. A circular region of interest (ROI) measuring 2 µm × 2 µm containing GFP was bleached with a 488 nm laser pulse (100% intensity) using a 63×/1.4 oil immersion objective lens. At least five granules from different roots were bleached and analyzed for each sample.

mRNA decay analysis

The mRNA decay analysis was conducted as previously described[17]. In brief, 5-day-old Col-0, *pat2-2* and *dcp5-1* mutant seedlings were pre-treated at 37 °C for 12 h and then incubated in 3 ml of incubation buffer (15 mM sucrose, 1 mM KCl, 1 mM PIPES pH 6.25, 1 mM sodium citrate) with rotation at 80 rpm in 24-well plates (Corning Costar) for 15 min. The bathing solution was replaced with 2 ml of fresh buffer containing 1 mM cordycepin (Solarbio, IC0920), followed by vacuum infiltration for 1 min. T_0 samples were immediately harvested and frozen in liquid N_2. The remaining samples underwent two additional rounds of 1-min vacuum infiltration, with 1-min decompression intervals. Samples incubated at 37 °C were collected at 15, 30 and 60 min after the first vacuum infiltration, frozen in liquid N_2 and subjected to total RNA isolation and RT-qPCR. Two independent biological replicates were performed with approximately 20 seedlings per sample in each replicate.

Heat stress tolerance assay

Heat stress tolerance assays were conducted as previously described[17]. Briefly, 5-day-old *Arabidopsis* seedlings grown on 1/2 MS plates in the growth chamber (Percival, CU-36L5) were subjected to heat stress at 44 °C for 105 min in an incubator (SPX-160, Ningbo, China). Following heat stress, the seedlings were recovered at 22 °C for 7 days in the growth chamber before measuring the survival rate. The survival rates

were calculated based on results from eight biological replicates, with at least 25 seedlings per genotype in each replicate.

Isolation of SGs fraction for ubiquitinome

Stress granules (SGs) were isolated as previously described[14] without the IP step. Briefly, 6-day-old *Arabidopsis* seedlings were harvested after heat stress and ground into fine powder using liquid nitrogen. 5 g of ground powder was mixed with 5 mL ice-cold SG extraction buffer [50 mM Tris-HCl pH 7.4, 100 mM potassium acetate, 2 mM magnesium acetate, 0.2% NP-40, 1 mM DTT, 1 mM NaF, 1 mM Na_3VO_4, protease inhibitor cocktail (Roche) with 50 μM PR-619 and 0.4 U/μl Rnase Inhibitor (Beyotime, R0102-10kU)] and incubated at 4 °C for 1 h. Subsequently, the homogenate was centrifuged at 4000 × *g* for 10 min at 4 °C to separate the supernatant and the pellet. The pellet was resuspended in 5 mL lysis buffer, vortexed, and centrifuged at 18,000 × *g* for 10 min at 4 °C. This process was repeated one time. After discarding the supernatant, the pellets were resuspended in 2 mL lysis buffer. Following a final centrifugation at 850 × *g* for 5 min at 4 °C, the supernatant was checked for the presence of SGs by confocal microscopy and used for ubiquitinome analysis.

The ubiquitinome was conducted by JingJie PTM Bio (Hangzhou, China) with the samples from three independent biological experiments. The protein sample was mixed with 1 volume of pre-cooled acetone, vortexed, and then precipitated with 4 volumes of pre-cooled acetone at −20 °C for 2 h. The precipitate was redissolved in 200 mM TEAB and dispersed ultrasonically. Trypsin was added at 1:50 trypsin-to-protein mass ratio for the first digestion overnight. The sample was then reduced with 5 mM dithiothreitol for 60 min at 37 °C and alkylated with 11 mM iodoacetamide for 45 min at room temperature in the dark. Finally, the peptides were desalted using Strata X SPE column.

To enrich modified peptides, tryptic peptides dissolved in NETN buffer (100 mM NaCl, 1 mM EDTA, 50 mM Tris-HCl, 0.5% NP-40, pH 8.0) were incubated with pre-washed antibody beads (Lot number PTM1104, PTM Bio) at 4 °C overnight with gentle shaking. The beads were washed for four times with NETN buffer and twice with H_2O. The bound peptides were eluted with 0.1% trifluoroacetic acid, and the eluted fractions were combined and vacuum-dried. Prior to LC-MS/MS analysis, the peptides were desalted using C18 ZipTips (Millipore) following the manufacturer's instructions.

Ubiquitinome data analysis

For the quantitative analysis of ubiquitinome, tryptic peptides were dissolved in solvent A (0.1% formic acid, 2% acetonitrile/in water) and directly loaded onto a custom-made reversed-phase analytical column (25-cm length, 100 μm i.d.). The mobile phase consisted of solvent A and solvent B (0.1% formic acid in acetonitrile). The peptides were separated using the following gradient: 0–18 min, 6–22%B; 18–22 min, 22–30%B; 22–26 min, 30–80%B; 26–30 min, 80%B, all at a constant flow rate of 450 nl/min on a NanoElute UHPLC system (Bruker Daltonics). The peptides were then subjected to capillary electrophoresis followed by mass spectrometry using the timsTOF Pro instrument. The electrospray voltage applied was 1.6 kV. Precursors and fragments were analyzed at the TOF detector, and the timsTOF Pro was operated in data-independent parallel accumulation serial fragmentation (diaPASEF) mode. The full MS scan range was set to 100–1700 (MS/MS scan range), with 8 PASEF (MS/MS mode) -MS/MS scans acquired per cycle, and the MS/MS scan range was set to 425–1025 m/z with an isolation window of 25 m/z.

To construct the spectral library and perform quantitative analysis, the DDA data were processed using Spectronaut (v.17.0) software coupled with Pulsar search engine. The tandem mass spectra were searched against Arabidopsis_thaliana_3702_PR_ 20230529.fasta (39320 entries) concatenated with reverse decoy database. The maximum number of missing cleavages was set to 4. Carbamidomethyl on Cys was specified as a fixed modification, while acetylation on protein N-terminal, oxidation on Met, and ubiquitylation were specified as variable modifications. The false discovery rate (FDR) of proteins, peptides and PSM were adjusted to less than 1%.

The raw LC-MS datasets were initially searched against database and converted into matrices representing the intensity of peptides across samples. Subsequently, the relative quantitative value of each modified peptide were calculated based on this intensity information using the following steps: 1) The intensities of modified peptides (*I*) were centralized, and transformed into relative quantitative values (*R*) using the formula *Rij* = *Iij* / *Mean(Ij)*, where *i* denotes the sample and *j* denotes the modified peptide. 2) If both Proteomics and post-translational modification profiling were conducted on the same cohort, the relative quantitative value of the modified peptide was further normalized by dividing it by the relative quantitative value of corresponding protein to mitigate the influence protein expression on modifications.

The fold change (FC) is defined as the ratio of the mean relative quantitative values of the modifier sites between two sample groups. For example, FC is calculated for comparing modifier sites between sample group A and sample group B using the following formula: $FC_{A/B,\ k}$ = Mean (R_{ik}, i ∈ A) / Mean (R_{ik}, i ∈ B), the R represents the relative quantitative value of the modifier site, the i denotes the sample, and the k denotes the specific modifier site.

To assess the statistical significance of these differences, the relative quantitative value of the modification site between two sample groups was tested by a two-tailed unpaired Student's *t* test. The resulting *P*-value serves as an indicator of significance, with a default threshold of $P < 0.05$. The T-test is performed on the Log_2-transformed relative quantitative values of the modifier sites from both groups. The Log_2 transformation is applied to ensure that the data meet the normal distribution requirement for the T-test. The calculation formula for *P*-value is as follows: P_k = T-test[$Log_2(R_{ik}$, i ∈ A), $Log_2(R_{ik}$, i ∈ B)]. The modification site with *P*-value < 0.05, Log_2(FC_HS/RC_5h) > 1 was regarded as significant up-regulated site, while the modification site with *P*-value < 0.05, Log_2(FC_HS/RC_5h) < −1 was regarded as significant down-regulated site.

Gene ontology enrichment analysis was conducted using Metascape[94] (https://metascape.org/gp/index.html#/main/step1).

Immunoblot assays

For the in vivo co-immunoprecipitation (co-IP), the experimental procedure was conducted as described above. The co-IP samples were separated using 8% or 10% (w/v) SDS-PAGE gels and transferred onto nitrocellulose filter membranes via electrophoresis. Protein gel blotting was conducted using the following primary antibodies: anti-GFP (Roche; 11814460001, 1:1000), anti-RFP (Chromotek; 5F8, 1:1000), anti-actin (ABclonal; AC009, 1:3000), anti-TSN (ABclonal; 1:4000), anti-AP-3β (ABclonal; 1:2000), anti-AP-3δ (ABclonal; 1:2000), anti-VPS18 (ABclonal; 1:2000)[28], anti-RPN1a (Agrisera; AS194264, 1:2000), anti-RPT2 (Agrisera; AS194262, 1:2000), anti-RPN5a (Agrisera; AS194265, 1:3000), anti-RPN12a (Agrisera; AS194268, 1:2000), anti-PAC1 (Agrisera; AS194258, 1:2000), anti-PBF1 (Agrisera; AS194261, 1:2000) and anti-PAG1 (Agrisera; AS194259, 1:3000). The following secondary antibodies were utilized: HRP-conjugated goat anti-mouse secondary antibody (Sangon; D110087, 1:5000), HRP-conjugated goat anti-rabbit secondary antibody (Sangon, D110058, 1:5000) and HRP-conjugated goat anti-rat secondary antibody (Sino Biological; SSA005, 1:5000).

For immunoblot analysis of the SGs fraction, the isolated SGs samples were run on 10% (w/v) SDS-PAGE gels and transferred onto nitrocellulose filter membranes via electrophoresis. Protein gel blotting was performed using the following primary antibodies: anti-Ubiquitin (Santa Cruz; sc-8017, 1:4000), anti-actin (ABclonal; AC009, 1:3000), anti-K48 ubiquitin (Cell Signaling Technology; #4289, 1:2000) and anti-K63 ubiquitin (EMD Millipore; 05-1308,

clone apu3, 1:3000) and the secondary antibodies as described above.

Proteasome activity and Ub-AMC hydrolysis assays

The proteasome activity was measured as previously described[95]. The substrate Suc-LLVY-AMC (GLPBIO, C3450) was employed to measure the proteasome activity. Briefly, an equal amount (50 μg) of protein from supernatants or the SGs fractions was added to a reaction buffer [50 mM Tris-HCl pH 7.5, 25 mM NaCl, 2 mM $MgCl_2$ and 5% glycerol] containing freshly prepared 2 mM dithiothreitol (DTT) and 5 mM adenosine triphosphate (ATP) in a total volume of 47.5 μL. The reaction mixture was then transferred to a 96-well plate and pre-incubated at 37 °C for 15 min in a microplate reader (Varioskan LUX, Thermo, USA50). The reaction was initiated by adding 2.5 μL of 2 mM Suc-LLVY-AMC to the final concentration of 100 μM. Fluorescence was recorded every 5 min for 90 min at 37 °C, with the excitation wavelength set at 360 nm and the emission wavelength at 460 nm. Each experiment was performed in triplicate, and the relative fold changes in fluorescence were calculated.

The Ub-AMC hydrolysis assay was conducted as previously described[96]. The substrate Ub-AMC (LifeSensors, LSS-SI220) was utilized to measure the deubiquitinase activity in SG fractions. Briefly, the SG fractions were resuspended in Ub-AMC assay buffer [50 mM Tris-HCl pH 7.5, 1 mM EDTA, 1 mg/mL ovalbumin, 2 mM $MgCl_2$] at the final step of the SG isolation. An equal amount (50 μg) of SG fractions was added to Ub-AMC assay buffer containing freshly prepared 2 mM DTT and 5 mM ATP, in a total volume of 47.5 μL. The reaction mixture was then transferred to a 96-well plate and pre-incubated at 37 °C for 15 min in a microplate reader (Varioskan LUX, Thermo, USA50). The reaction was initiated by adding 2.5 μL of 10 μM Ub-AMC to the final concentration of 500 nM. The fluorescence was recorded every 5 min for 90 min at 37 °C, with the excitation wavelength set at 380 nm and the emission wavelength at 460 nm. Each experiment was performed in triplicate, and the relative fold changes in fluorescence were calculated.

Transient expression analysis in protoplasts

The vectors *ProUBQ::UBP6-GFP* and *Pro35S::RFP-RBP47b*, used for protoplast transformation, were described above. *Arabidopsis* protoplasts were obtained as outlined in a previous study[97]. Briefly, leaves were collected from 4-week-old wild type and *tsn1tsn2* double mutant plants, peeled, and subjected to enzyme digestion (1.5% [w/v] cellulase R10 [Yakult, 180612-02], 0.4% [w/v] macerozyme R10 [Yakult, 170106-01], 0.4 M mannitol, 10 mM $CaCl_2$, 20 mM KCl, 0.1% [w/v] BSA, and 20 mM MES, pH 5.7). The protoplasts were washed with W5 solution (154 mM NaCl, 125 mM $CaCl_2$, 5 mM KCl, 5 mM glucose, and 2 mM MES, pH 5.7) and resuspended in MMG solution (0.4 M mannitol, 15 mM $MgCl_2$, and 4 mM MES, pH 5.7). Subsequently, they were mixed with PEG-calcium transfection solution (30% [w/v] PEG4000, 0.2 M mannitol, and 100 mM $CaCl_2$) and 10 μg of desired plasmids for transformation. The transformed protoplasts were incubated in W5 solution under low-light condition for 16 h before confocal analysis using a Leica SP8 confocal system.

Surface sensing of translation (SUnSET) assay

The SUnSET assay was conducted based on previous reports with minor modifications[57,58]. 5-day-old seedlings were immersed in 2 ml 1/2 liquid medium containing 60 μM puromycin at room temperature (RT) or under heat stress (HS) (39 °C, water bath) for 40 min. For recovery, the heat-stressed seedlings were transferred to a new 2 ml 1/2 liquid medium, and puromycin was added to co-incubate for 40 min before the end of indicated recovery time. After the puromycin treatment, the seedlings were rinsed twice with water, blotted dry, and subsequently ground into fine powder in liquid nitrogen. The powder was then homogenized in protein extraction buffer [50 mM Tris-HCl (pH 7.5), 150 mM NaCl, 0.1% NP-40, 10 mM DTT, 1 μM PMSF and 1× protease inhibitor cocktail (Roche, 11836170001)]. The supernatants were isolated by centrifuging at 16,000 × *g* at 4 °C for 15 min and adjusted to equal protein concentrations for SDS-PAGE electrophoresis. Newly synthesized proteins were detected using immunoblot with an anti-puromycin antibody (Millipore Sigma; MABE343, 1:10000) and HRP-conjugated goat anti-mouse secondary antibody (Sangon; D110087, 1:5000). The intensities of bands were quantified using Image J software.

Polysome profiles

Polysome profiles were conducted as described previously[98]. 6-day-old seedlings were heat-stressed and recovered as outlined above. Subsequently, the samples were pulverized finely in liquid nitrogen. Approximately 400 mg of tissue powder were further homogenized with 1.2 mL of lysis buffer [200 mM Tris-HCl, pH 9.0, 200 mM KCl, 25 mM EGTA, 35 mM $MgCl_2$, 1% detergent mix [1% Tween 20, 1% Triton, 1% Brij35, and 1% Igepal-CA630], 1% sodium deoxycholate, 1% polyoxyethylene tridecyl ether, 5 mM DTT, 1 mM PMSF, 100 μg/mL cycloheximide, 50 μg/mL chloramphenicol, 100 U/ml RNase inhibitor (Vazyme, R301-03) and 1× protease inhibitor cocktail (Roche)]. The homogenate was incubated on ice for 30 min. Following centrifugation at 16,000 × *g* at 4 °C for 15 min, the supernatant was clarified using a 0.22-μm low protein binding filter (Beyotime, FF372) and measured at $OD_{260\ nm}$ with Nanodrop. Subsequently, all samples with the same amount of $OD_{260\ nm}$ were loaded onto a 10–60% sucrose gradient (11 mL). Ultracentrifugation was performed using a SW41 rotor at 38,000 rpm for 3 h. Polysome profiles analyses were performed with a BioComp absorbance detector at 260 nm. For normalization and direct comparison of profiles, equal amounts of filtered-supernatant from each sample were loaded onto the sucrose gradient. The percentage of polysomes for each sample was determined using GraphPad Prism 8.0 as the ratio between polysomes area and total area (including the 40S, 60S, monosome and polysome areas).

Image analysis

Fluorescence colocalization analysis were performed using ImageJ software (https://imagej.net/Fiji.html) with the Pearson correlation coefficients (PCC) plug-in (http://www.cpib.ac.uk/~afrench/coloc.html)[99]. First, the Split channels function in ImageJ was used to split the merged fluorescence image, and then the PCC plugin was used to calculate the Pearson coefficients of the green and red channels using the default parameters of the software. PCC values fell within a range from −1 (representing negative correlations) to +1 (representing positive correlations). SGs with the size above 0.1 μm were scored as positive. The counting of SGs was conducted using the "Analyze >> Analyze Particles" plug-in in ImageJ with equal area across images. The foci size was measured automatically using ImageJ. The displayed values are averages derived from at least three separate biological experiments.

Statistics and reproducibility

Statistical differences (*P*-value) were calculated a two-tailed unpaired Student's *t* test using Microsoft Excel or one-way analysis of variance (ANOVA) with Tukey's multiple comparison test by GraphPad Prism software (version 8.0.1). The statistical analysis for each experiment is described in the figure legends. The P value < 0.05 was considered to indicate statistical significance. For representative data of western bolt such as Figs. 1b, e, 2l, m, 3d, 5a, c, 6c, e, f, h, 7e, c and Supplementary Figs. 1a, b, c, 2a, b, 6e–h, 12g, h, 14h, i, 15a, b, d, f, h, j and 17a, c, at least two biological replications were shown, each time were observed with the similar result. For representative data of confocal observation experiments such as Figs. 2a, c, e, g, i, 3e, g, i, k, m, o, q, s, 4a, d, 5d, f, i, k and 6a and Supplementary Figs. 3a–c, f, g, j, k, 4c, d, 5e, 7a, 9a, c, 10a, b, 11a, 13b, 14a–e and 16d, at least three biological replications

were shown, each time at least five different seedlings were observed with the similar result. For representative data of SUC-LLVY-AMC assay such as Fig. 5h and Supplementary Fig. 11c or Ub-AMC assay such as Fig. 6j, k and Supplementary Fig. 15n, one representative replicate of three biological replications were shown, each biological replication were observed with the similar result.

Reporting summary

Further information on research design is available in the Nature Portfolio Reporting Summary linked to this article.

Data availability

All materials in this study are available from the corresponding author upon request. The raw data of AP-3β interactome and SGs ubiquitinome have been deposited to the ProteomeXchange Consortium via the PRIDE partner repository with the dataset identifier PXD054299 and PXD058194, respectively. The main data supporting the findings of this study are available within the article and its Supplementary Information. The source data underlying Figs. 1–7, Supplementary Figs. 1–17 are provided as a Source Data file. Protein list of AP-3β interactome identified by LC-MS is provided in Supplementary Data 1; protein list for Venn diagram and GO enrichment analysis is provided in Supplementary Data 2; primer sequences are provided in Supplementary Data 3; data information in ubiquitinome is provided in Supplementary Data 4. Source data are provided with this paper.

References

1. Chantarachot, T. & Bailey-Serres, J. Polysomes, Stress Granules, and Processing Bodies: A Dynamic Triumvirate Controlling Cytoplasmic mRNA Fate and Function. *Plant Physiol.* **176**, 254–269 (2018).
2. Solis-Miranda, J. et al. Stress-related biomolecular condensates in plants. *Plant Cell* **35**, 3187–3204 (2023).
3. Maruri-Lopez, I., Figueroa, N. E., Hernandez-Sanchez, I. E. & Chodasiewicz, M. Plant Stress Granules: Trends and Beyond. *Front. Plant Sci.* **12**, 722643 (2021).
4. Kassouf, T. et al. Targeting the NEDP1 enzyme to ameliorate ALS phenotypes through stress granule disassembly. *Sci. Adv.* **9**, eabq7585 (2023).
5. Cereghetti, G. et al. Reversible amyloids of pyruvate kinase couple cell metabolism and stress granule disassembly. *Nat. Cell Biol.* **23**, 1085–1094 (2021).
6. Buchan, J. R., Kolaitis, R. M., Taylor, J. P. & Parker, R. Eukaryotic stress granules are cleared by autophagy and Cdc48/VCP function. *Cell* **153**, 1461–1474 (2013).
7. Wang, F. et al. SERBP1 Promotes Stress Granule Clearance by Regulating 26S Proteasome Activity and G3BP1 Ubiquitination and Protects Male Germ Cells from Thermostimuli Damage. *Research* **6**, 0091 (2023).
8. Turakhiya, A. et al. ZFAND1 Recruits p97 and the 26S Proteasome to Promote the Clearance of Arsenite-Induced Stress Granules. *Mol. Cell* **70**, 906–919 e907 (2018).
9. Maxwell, B. A. et al. Ubiquitination is essential for recovery of cellular activities after heat shock. *Science* **372**, eabc3593 (2021).
10. Tolay, N. & Buchberger, A. Comparative profiling of stress granule clearance reveals differential contributions of the ubiquitin system. *Life Sci. Alliance* **4**, e202000927 (2021).
11. Gwon, Y. et al. Ubiquitination of G3BP1 mediates stress granule disassembly in a context-specific manner. *Science* **372**, eabf6548 (2021).
12. Pan, C. R., Knutson, S. D., Huth, S. W. & MacMillan D. W. C. microMap proximity labeling in living cells reveals stress granule disassembly mechanisms. *Nat. Chem. Biol.* https://www.nature.com/articles/s41589-024-01721-2 (2024).
13. Gutierrez-Beltran, E., Moschou, P. N., Smertenko, A. P. & Bozhkov, P. V. Tudor staphylococcal nuclease links formation of stress granules and processing bodies with mRNA catabolism in Arabidopsis. *Plant Cell* **27**, 926–943 (2015).
14. Kosmacz, M. et al. Protein and metabolite composition of Arabidopsis stress granules. *N. Phytol.* **222**, 1420–1433 (2019).
15. Palanivelu, R., Belostotsky, D. A. & Meagher, R. B. Arabidopsis thaliana poly (A) binding protein 2 (PAB2) functions in yeast translational and mRNA decay processes. *Plant J.* **22**, 187–198 (2000).
16. Nguyen, C. C. et al. Oligouridylate Binding Protein 1b Plays an Integral Role in Plant Heat Stress Tolerance. *Front. Plant Sci.* **7**, 853 (2016).
17. Tong, J. et al. ALBA proteins confer thermotolerance through stabilizing HSF messenger RNAs in cytoplasmic granules. *Nat. Plants* **8**, 778–791 (2022).
18. Zhu, S. et al. Liquid-liquid phase separation of RBGD2/4 is required for heat stress resistance in Arabidopsis. *Dev. Cell* **57**, 583–597 e586 (2022).
19. McLoughlin, F., Kim, M., Marshall, R. S., Vierstra, R. D. & Vierling, E. HSP101 Interacts with the Proteasome and Promotes the Clearance of Ubiquitylated Protein Aggregates. *Plant Physiol.* **180**, 1829–1847 (2019).
20. Xie, Z. et al. Proteasome resides in and dismantles plant heat stress granules constitutively. *Mol. Cell* **84**, 3320–3335 e3327 (2024).
21. Odorizzi, G., Cowles, C. R. & Emr, S. D. The AP-3 complex: a coat of many colours. *Trends Cell Biol.* **8**, 282–288 (1998).
22. Ma, Z., Islam, M. N., Xu, T. & Song, E. AP-3 adaptor complex-mediated vesicle trafficking. *Biophys. Rep.* **7**, 91–100 (2021).
23. Peden, A. A. et al. Localization of the AP-3 adaptor complex defines a novel endosomal exit site for lysosomal membrane proteins. *J. Cell Biol.* **164**, 1065–1076 (2004).
24. Zwiewka, M. et al. The AP-3 adaptor complex is required for vacuolar function in Arabidopsis. *Cell Res.* **21**, 1711–1722 (2011).
25. Feraru, E. et al. The AP-3 beta adaptin mediates the biogenesis and function of lytic vacuoles in Arabidopsis. *Plant Cell* **22**, 2812–2824 (2010).
26. Feng, Q. N. et al. Adaptor Protein-3-Dependent Vacuolar Trafficking Involves a Subpopulation of COPII and HOPS Tethering Proteins. *Plant Physiol.* **174**, 1609–1620 (2017).
27. Gutierrez-Beltran, E. et al. Tudor staphylococcal nuclease is a docking platform for stress granule components and is essential for SnRK1 activation in Arabidopsis. *EMBO J.* **40**, e105043 (2021).
28. Jiang, D. et al. Arabidopsis HOPS subunit VPS41 carries out plant-specific roles in vacuolar transport and vegetative growth. *Plant Physiol.* **189**, 1416–1434 (2022).
29. Yan, C., Yan, Z., Wang, Y., Yan, X. & Han, Y. Tudor-SN, a component of stress granules, regulates growth under salt stress by modulating GA20ox3 mRNA levels in Arabidopsis. *J. Exp. Bot.* **65**, 5933–5944 (2014).
30. Geldner, N. et al. Rapid, combinatorial analysis of membrane compartments in intact plants with a multicolor marker set. *Plant J.* **59**, 169–178 (2009).
31. Pang, L. et al. The small GTPase RABA2a recruits SNARE proteins to regulate the secretory pathway in parallel with the exocyst complex in Arabidopsis. *Mol. Plant* **15**, 398–418 (2022).
32. Bu, F., Yang, M., Guo, X., Huang, W. & Chen, L. Multiple Functions of ATG8 Family Proteins in Plant Autophagy. *Front. Cell Dev. Biol.* **8**, 466 (2020).
33. Emans, N., Zimmermann, S. & Fischer, R. Uptake of a fluorescent marker in plant cells is sensitive to brefeldin A and wortmannin. *Plant Cell* **14**, 71–86 (2002).
34. Kedersha, N. et al. Stress granules and processing bodies are dynamically linked sites of mRNP remodeling. *J. Cell Biol.* **169**, 871–884 (2005).

35. Zheng, W. et al. AP3M harbors actin filament binding activity that is crucial for vacuole morphology and stomatal closure in Arabidopsis. *Proc. Natl Acad. Sci. USA* **116**, 18132–18141 (2019).
36. Ivanov, P., Kedersha, N. & Anderson, P. Stress Granules and Processing Bodies in Translational Control. *Cold Spring Harb. Perspect. Biol.* **11**, a032813 (2019).
37. Xu, J. & Chua, N. H. Arabidopsis decapping 5 is required for mRNA decapping, P-body formation, and translational repression during postembryonic development. *Plant Cell* **21**, 3270–3279 (2009).
38. Yang, C. et al. Stress granule homeostasis is modulated by TRIM21-mediated ubiquitination of G3BP1 and autophagy-dependent elimination of stress granules. *Autophagy* **19**, 1934–1951 (2023).
39. Lee, K. H. et al. The RPT2 subunit of the 26S proteasome directs complex assembly, histone dynamics, and gametophyte and sporophyte development in Arabidopsis. *Plant Cell* **23**, 4298–4317 (2011).
40. Book, A. J. et al. Affinity purification of the Arabidopsis 26 S proteasome reveals a diverse array of plant proteolytic complexes. *J. Biol. Chem.* **285**, 25554–25569 (2010).
41. Al-Shami, A. et al. Regulators of the proteasome pathway, Uch37 and Rpn13, play distinct roles in mouse development. *Plos One* **5**, e13654 (2010).
42. Chen, P. C. et al. The proteasome-associated deubiquitinating enzyme Usp14 is essential for the maintenance of synaptic ubiquitin levels and the development of neuromuscular junctions. *J. Neurosci.* **29**, 10909–10919 (2009).
43. Hanna, J. et al. Deubiquitinating enzyme Ubp6 functions noncatalytically to delay proteasomal degradation. *Cell* **127**, 99–111 (2006).
44. de Poot, S. A. H., Tian, G. & Finley, D. Meddling with Fate: The Proteasomal Deubiquitinating Enzymes. *J. Mol. Biol.* **429**, 3525–3545 (2017).
45. Shin, J. Y. et al. Deubiquitination Reactions on the Proteasome for Proteasome Versatility. *Int. J. Mol. Sci.* **21**, 5312 (2020).
46. Kandolf, S. et al. Cryo-EM structure of the plant 26S proteasome. *Plant Commun.* **3**, 100310 (2022).
47. Altun, M. et al. Activity-based chemical proteomics accelerates inhibitor development for deubiquitylating enzymes. *Chem. Biol.* **18**, 1401–1412 (2011).
48. Kapuria, V. et al. Deubiquitinase inhibition by small-molecule WP1130 triggers aggresome formation and tumor cell apoptosis. *Cancer Res.* **70**, 9265–9276 (2010).
49. Li, J. et al. Capzimin is a potent and specific inhibitor of proteasome isopeptidase Rpn11. *Nat. Chem. Biol.* **13**, 486–493 (2017).
50. D'Arcy, P. et al. Inhibition of proteasome deubiquitinating activity as a new cancer therapy. *Nat. Med.* **17**, 1636–1640 (2011).
51. Skelly, M. J., Furniss, J. J., Grey, H., Wong, K. W. & Spoel, S. H. Dynamic ubiquitination determines transcriptional activity of the plant immune coactivator NPR1. *Elife* **8**, e47005 (2019).
52. Tian, G., Lu, Q., Kohalmi, S. E., Rothstein, S. J. & Cui, Y. Evidence that the Arabidopsis Ubiquitin C-terminal Hydrolases 1 and 2 associate with the 26S proteasome and the TREX-2 complex. *Plant Signal Behav.* **7**, 1415–1419 (2012).
53. Feng, H., Tan, J. & Deng, Z. Decoding plant adaptation: deubiquitinating enzymes UBP12 and UBP13 in hormone signaling, light response, and developmental processes. *J. Exp. Bot.* **75**, 721–732 (2024).
54. Yu, H. & Matouschek, A. Recognition of Client Proteins by the Proteasome. *Annu. Rev. Biophys.* **46**, 149–173 (2017).
55. Lee, B. H. et al. USP14 deubiquitinates proteasome-bound substrates that are ubiquitinated at multiple sites. *Nature* **532**, 398–401 (2016).
56. Zhang, S. et al. USP14-regulated allostery of the human proteasome by time-resolved cryo-EM. *Nature* **605**, 567–574 (2022).
57. Schmidt, E. K., Clavarino, G., Ceppi, M. & Pierre, P. SUnSET, a nonradioactive method to monitor protein synthesis. *Nat. Methods* **6**, 275–277 (2009).
58. Karunadasa, S. S., Kurepa, J., Shull, T. E. & Smalle, J. A. Cytokinin-induced protein synthesis suppresses growth and osmotic stress tolerance. *N. Phytol.* **227**, 50–64 (2020).
59. Lippincott-Schwartz, J., Yuan, L. C., Bonifacino, J. S. & Klausner, R. D. Rapid redistribution of Golgi proteins into the ER in cells treated with brefeldin A: evidence for membrane cycling from Golgi to ER. *Cell* **56**, 801–813 (1989).
60. Nebenfuhr, A., Ritzenthaler, C. & Robinson, D. G. Brefeldin A: deciphering an enigmatic inhibitor of secretion. *Plant Physiol.* **130**, 1102–1108 (2002).
61. Wang, J., Cai, Y., Miao, Y., Lam, S. K. & Jiang, L. Wortmannin induces homotypic fusion of plant prevacuolar compartments. *J. Exp. Bot.* **60**, 3075–3083 (2009).
62. Nascimbeni, A. C., Codogno, P. & Morel, E. Phosphatidylinositol-3-phosphate in the regulation of autophagy membrane dynamics. *FEBS J.* **284**, 1267–1278 (2017).
63. Haas, T. J. et al. The Arabidopsis AAA ATPase SKD1 is involved in multivesicular endosome function and interacts with its positive regulator LYST-INTERACTING PROTEIN5. *Plant Cell* **19**, 1295–1312 (2007).
64. Wolff, H., Jakoby, M., Stephan, L., Koebke, E. & Hulskamp, M. Heat Stress-Dependent Association of Membrane Trafficking Proteins With mRNPs Is Selective. *Front. Plant Sci.* **12**, 670499 (2021).
65. Tse, Y. C. et al. Identification of multivesicular bodies as prevacuolar compartments in Nicotiana tabacum BY-2 cells. *Plant Cell* **16**, 672–693 (2004).
66. Saad, S. et al. Reversible protein aggregation is a protective mechanism to ensure cell cycle restart after stress. *Nat. Cell Biol.* **19**, 1202–1213 (2017).
67. Ramaswami, M., Taylor, J. P. & Parker, R. Altered ribostasis: RNA-protein granules in degenerative disorders. *Cell* **154**, 727–736 (2013).
68. Liu, C. et al. SEC14-like condensate phase transitions at plasma membranes regulate root growth in Arabidopsis. *Plos Biol.* **21**, e3002305 (2023).
69. Dragwidge, J. M. & Van Damme, D. Protein phase separation in plant membrane biology: more than just a compartmentalization strategy. *Plant Cell* **35**, 3162–3172 (2023).
70. Liu, C. et al. An actin remodeling role for Arabidopsis processing bodies revealed by their proximity interactome. *EMBO J.* **42**, e111885 (2023).
71. Liu, C. et al. A proxitome-RNA-capture approach reveals that processing bodies repress coregulated hub genes. *Plant Cell* **36**, 559–584 (2024).
72. Gonzalez, F., Delahodde, A., Kodadek, T. & Johnston, S. A. Recruitment of a 19S proteasome subcomplex to an activated promoter. *Science* **296**, 548–550 (2002).
73. Ferdous, A., Gonzalez, F., Sun, L., Kodadek, T. & Johnston, S. A. The 19S regulatory particle of the proteasome is required for efficient transcription elongation by RNA polymerase II. *Mol. Cell* **7**, 981–991 (2001).
74. Cheon, Y., Kim, H., Park, K., Kim, M. & Lee, D. Dynamic modules of the coactivator SAGA in eukaryotic transcription. *Exp. Mol. Med.* **52**, 991–1003 (2020).
75. Ezhkova, E. & Tansey, W. P. Proteasomal ATPases link ubiquitylation of histone H2B to methylation of histone H3. *Mol. Cell* **13**, 435–442 (2004).
76. Seo, H. D. et al. The 19S proteasome is directly involved in the regulation of heterochromatin spreading in fission yeast. *J. Biol. Chem.* **292**, 17144–17155 (2017).
77. Sun, C. et al. An abundance of free regulatory (19S) proteasome particles regulates neuronal synapses. *Science* **380**, eadf2018 (2023).
78. Roelofs, J. et al. Chaperone-mediated pathway of proteasome regulatory particle assembly. *Nature* **459**, 861–865 (2009).

79. Nathan, J. A., Kim, H. T., Ting, L., Gygi, S. P. & Goldberg, A. L. Why do cellular proteins linked to K63-polyubiquitin chains not associate with proteasomes? *EMBO J.* **32**, 552–565 (2013).
80. Guo, N. & Peng, Z. MG132, a proteasome inhibitor, induces apoptosis in tumor cells. *Asia Pac. J. Clin. Oncol.* **9**, 6–11 (2013).
81. Park, H. S., Jun do, Y., Han, C. R., Woo, H. J. & Kim, Y. H. Proteasome inhibitor MG132-induced apoptosis via ER stress-mediated apoptotic pathway and its potentiation by protein tyrosine kinase p56lck in human Jurkat T cells. *Biochem. Pharm.* **82**, 1110–1125 (2011).
82. Gurtovenko, A. A. & Anwar, J. Modulating the structure and properties of cell membranes: the molecular mechanism of action of dimethyl sulfoxide. *J. Phys. Chem. B* **111**, 10453–10460 (2007).
83. Sauer, M., Paciorek, T., Benkova, E. & Friml, J. Immunocytochemical techniques for whole-mount in situ protein localization in plants. *Nat. Protoc.* **1**, 98–103 (2006).
84. Back, S., Gorman, A. W., Vogel, C. & Silva, G. M. Site-Specific K63 Ubiquitinomics Provides Insights into Translation Regulation under Stress. *J. Proteome Res.* **18**, 309–318 (2019).
85. Silva, G. M., Finley, D. & Vogel, C. K63 polyubiquitination is a new modulator of the oxidative stress response. *Nat. Struct. Mol. Biol.* **22**, 116–123 (2015).
86. Romero-Barrios, N. & Vert, G. Proteasome-independent functions of lysine-63 polyubiquitination in plants. *N. Phytol.* **217**, 995–1011 (2018).
87. Ichikawa, M. et al. Syntaxin of plant proteins SYP123 and SYP132 mediate root hair tip growth in Arabidopsis thaliana. *Plant Cell Physiol.* **55**, 790–800 (2014).
88. Sorenson, R. & Bailey-Serres, J. Selective mRNA sequestration by OLIGOURIDYLATE-BINDING PROTEIN 1 contributes to translational control during hypoxia in Arabidopsis. *Proc. Natl Acad. Sci. USA* **111**, 2373–2378 (2014).
89. Wang, Z. et al. A cytoplasmic osmosensing mechanism mediated by molecular crowding-sensitive DCP5. *Science* **386**, eadk9067 (2024).
90. Yao, C., Wu, Y., Nie, H. & Tang, D. RPN1a, a 26S proteasome subunit, is required for innate immunity in Arabidopsis. *Plant J.* **71**, 1015–1028 (2012).
91. Grefen, C. et al. A ubiquitin-10 promoter-based vector set for fluorescent protein tagging facilitates temporal stability and native protein distribution in transient and stable expression studies. *Plant J.* **64**, 355–365 (2010).
92. Liu, G. et al. The deubiquitinases UBP12 and UBP13 integrate with the E3 ubiquitin ligase XBAT35.2 to modulate VPS23A stability in ABA signaling. *Sci. Adv.* **8**, eabl5765 (2022).
93. Grefen, C. & Blatt, M. R. A 2in1 cloning system enables ratiometric bimolecular fluorescence complementation (rBiFC). *Biotechniques* **53**, 311–314 (2012).
94. Zhou, Y. et al. Metascape provides a biologist-oriented resource for the analysis of systems-level datasets. *Nat. Commun.* **10**, 1523 (2019).
95. Han, J. J. et al. The beta5 subunit is essential for intact 26S proteasome assembly to specifically promote plant autotrophic growth under salt stress. *N. Phytol.* **221**, 1359–1368 (2019).
96. Hung, K. Y. S. et al. Allosteric control of Ubp6 and the proteasome via a bidirectional switch. *Nat. Commun.* **13**, 838 (2022).
97. Yoo, S. D., Cho, Y. H. & Sheen, J. Arabidopsis mesophyll protoplasts: a versatile cell system for transient gene expression analysis. *Nat. Protoc.* **2**, 1565–1572 (2007).
98. Merret, R. et al. Heat Shock Protein HSP101 Affects the Release of Ribosomal Protein mRNAs for Recovery after Heat Shock. *Plant Physiol.* **174**, 1216–1225 (2017).
99. French, A. P., Mills, S., Swarup, R., Bennett, M. J. & Pridmore, T. P. Colocalization of fluorescent markers in confocal microscope images of plant cells. *Nat. Protoc.* **3**, 619–628 (2008).

Acknowledgements

We sincerely thank Prof. Feifei Yu (China Agricultural University, China) for providing the pCAMBIA1300-*pro35S:UBP12-FLAG* vector. We also thank Prof. Hongwei Guo (Southern University of Science and Technology, China) for thoughtful discussion with the project and comments on the manuscript. R.L.is financially supported by grants from the National Natural Science Foundation of China (32270295, 32070193), and the Shenzhen Sci-Tech Fund (JCYJ20210324105004011 and 20220815103813001); L.P. is supported by grants from the National Natural Science Foundation of China (32270305). This work is supported by Shenzhen Science and Technology Program (Grant No. ZDSYS20230626091659010).

Author contributions

L.P. and R.L. designed the experiments. L.P., Y.Z.H., Y.L.H, and D.J. performed the experiments and analyzed the data. L.P. and R.L. wrote the manuscript.

Competing interests

The authors declare no competing interests.

Additional information

Supplementary information The online version contains supplementary material available at https://doi.org/10.1038/s41467-025-57306-7.

Correspondence and requests for materials should be addressed to Ruixi Li.

Peer review information *Nature Communications* thanks Panagiotis Moschou and the other, anonymous, reviewer(s) for their contribution to the peer review of this work. A peer review file is available.